

# OH and HO<sub>2</sub> radical chemistry in a midlatitude forest: Measurements and model comparisons

Michelle M. Lew<sup>1\*</sup>, Pamela S. Rickly<sup>2\*\*</sup>, Brandon P. Bottorff<sup>1</sup>, Emily Reidy<sup>1</sup>, Sofia Sklaveniti<sup>2,3</sup>, Thierry Léonardis<sup>3</sup>, Nadine Locoge<sup>3</sup>, Sebastien Dusanter<sup>3</sup>, Shuvashish Kundu<sup>4\*\*\*</sup>, Ezra Wood<sup>5</sup>, and Philip S. Stevens<sup>1,2</sup>

<sup>1</sup> Department of Chemistry, Indiana University, Bloomington, IN 47405, USA

<sup>2</sup> O'Neill School of Public and Environmental Affairs, Indiana University, Bloomington, IN 47405, USA

<sup>3</sup> IMT Lille Douai, Univ. Lille, SAGE – Département Sciences de l'Atmosphère et Génie de l'Environnement, 59000 Lille, France

<sup>4</sup> Department of Chemistry, University of Massachusetts - Amherst, Amherst, MA 01003, USA

<sup>5</sup> Department of Chemistry, Drexel University, Philadelphia, PA 19104, USA

\* now at California Air Resources Board, Sacramento, CA 95812, USA

\*\* now at Cooperative Institute for Research in Environmental Sciences, University of Colorado, Boulder, CO 80309, USA and Chemical Sciences Division, Earth System Research Laboratory, National Oceanic and Atmospheric Administration, Boulder, CO 80305, USA

\*\*\* now at Momentive Performance Materials, Inc., Tarrytown, NY 10591, United States

*Correspondence:* Philip S. Stevens ([pstevens@indiana.edu](mailto:pstevens@indiana.edu))

**Abstract.** Reactions of the hydroxyl (OH) and peroxy radicals (HO<sub>2</sub> and RO<sub>2</sub>) play a central role in the chemistry of the atmosphere. In addition to controlling the lifetimes of many trace gases important to issues of global climate change, OH radical reactions initiate the oxidation of volatile organic compounds (VOCs) which can lead to the production of ozone and secondary organic aerosols in the atmosphere. Previous measurements of these radicals in forest environments characterized by high mixing ratios of isoprene and low mixing ratios of nitrogen oxides (NO<sub>x</sub>) (typically less than 1-2 ppb) have shown serious discrepancies with modeled concentrations. These results bring into question our understanding of the atmospheric chemistry of isoprene and other biogenic VOCs under low NO<sub>x</sub> conditions.

During the summer of 2015, OH and HO<sub>2</sub> radical concentrations as well as total OH reactivity were measured using Laser-Induced Fluorescence - Fluorescence Assay by Gas Expansion (LIF-FAGE) techniques as part of the Indiana Radical, Reactivity and Ozone Production Intercomparison (IRRONIC). This campaign took place in a forested area near the Indiana University, Bloomington campus characterized by high mixing ratios of isoprene and low mixing ratios of NO<sub>x</sub>. Supporting measurements of photolysis rates, VOCs, NO<sub>x</sub>, and other species were used to constrain a zero-dimensional box model based on the Regional Atmospheric Chemistry Mechanism (RACM2) and the Master Chemical Mechanism (MCM). Using an OH chemical scavenger technique, the study revealed the presence of an interference with the LIF-FAGE measurements of OH that increased with both ambient concentrations of ozone and temperature. Subtraction of the interference resulted in measured OH concentrations (approximately 4×10<sup>6</sup> cm<sup>-3</sup> average daytime maximum) that were in better agreement with model

predictions, although the model still underestimated the measured concentrations, likely due to an underestimation of the concentration of NO at this site. Measurements of HO<sub>2</sub> concentrations during the campaign (approximately 1×10<sup>9</sup> cm<sup>-3</sup> average daytime maximum) included a fraction of isoprene-based peroxy radicals (HO<sub>2</sub>\*=HO<sub>2</sub> + αRO<sub>2</sub>) and were found to agree with model predictions to within 20%. On average, the measured reactivity was consistent with that calculated from measured OH sinks to within 20%, with modeled oxidation products accounting for the missing reactivity, although significant missing reactivity (approximately 40% of the total measured reactivity) was observed on some days.

## 1 Introduction

The hydroxyl radical (OH) is one of the primary oxidants in the atmosphere (Levy, 1972). The OH radical initiates the oxidation of volatile organic compounds (VOCs) that leads to the production of hydroperoxy radicals (HO<sub>2</sub>) and organic peroxy radicals (RO<sub>2</sub>). In the presence of nitrogen oxides (NO<sub>x</sub> = NO + NO<sub>2</sub>), reactions of these radicals can lead to the production of ozone and secondary organic aerosols in the atmosphere, the primary components of photochemical smog. Because of their short atmospheric lifetimes, measurements of OH and HO<sub>2</sub> (together HO<sub>x</sub>) and total OH reactivity can provide a robust test of our understanding of this complex chemistry (Heard and Pilling, 2003).

Multiple field campaigns have been conducted over the years measuring OH and HO<sub>2</sub> radicals in both urban and forested environments. Measurements of OH in urban areas characterized by high mixing ratios of NO<sub>x</sub> and anthropogenic VOCs have been generally consistent with model predictions (Ren et al., 2003; Shirley et al., 2006; Kanaya et al., 2007a; Dusanter et al., 2009b; Hofzumahaus et al., 2009; Griffith et al., 2016; Tan et al., 2017; 2018; 2019), while measurements in remote forested environments characterized by low mixing ratios of NO<sub>x</sub> and high mixing ratios of biogenic VOCs have often been greater than model predictions (Tan et al., 2001; Lelieveld et al., 2008; Whalley et al., 2011; Rohrer et al., 2014).

However, recent measurements by Mao et al. (2012) in a northern California forest using a new chemical scavenging technique that removes ambient OH before air enters the detection cell revealed a significant interference associated with their Laser-Induced Fluorescence (LIF) measurements of OH. The unknown interference was a factor of 2 to 3 times higher than ambient OH concentrations (Mao et al., 2012). Similar results were observed in a boreal forest by Novelli et al. (2014), who observed an interference using a similar chemical scrubbing technique that was a factor of 3 to 4 times higher than ambient OH concentrations. One possible source of this observed interference may be the decomposition of Criegee intermediates produced from the ozonolysis of biogenic emissions in the low-pressure detection cells used by LIF instruments, although the ambient concentration of these intermediates in the atmosphere may be too low to explain all of the observed interference (Novelli et al., 2017; Rickly and Stevens, 2018). Another proposed source of the interference is the decomposition of ROOOH molecules inside the FAGE detection cell formed from the reaction of OH with RO<sub>2</sub> radicals (Fittschen et al., 2019). Nevertheless, interferences associated with measurements of OH could explain part of the discrepancies between measured and modeled OH concentrations in forested environments. Monitoring potential interferences associated with OH measurements using LIF techniques may be crucial for understanding the discrepancies between measurements and models.

In contrast to measurements of OH, the agreement between measured and modeled HO<sub>2</sub> concentrations have been highly variable. In urban environments, measured HO<sub>2</sub> concentrations were sometimes found to agree with model predictions (Shirley et al., 2006; Emmerson et al., 2007; Dusanter et al., 2009b; Michoud et al., 2012; Lu et al., 2013; Ren et al., 2013; Griffith et al., 2016; Tan et al., 2017), while other times the measurements were found to be both lower (George et al., 1999; Konrad et al., 2003) and higher than model predictions (Martinez et al., 2003; Ren et al., 2003; Emmerson et al., 2005; Kanaya et al., 2007a; Chen et al., 2010; Sheehy et al., 2010; Czader et al., 2013; Griffith et al., 2016; Tan et al., 2018). In forested environments, measured HO<sub>2</sub> concentrations were sometimes found to agree with model predictions (Tan, D. et al., 2001; Ren et al., 2005; 2006), but were often found to be either lower (Carslaw et al., 2001; Kanaya et al., 2007b; Whalley et al., 2011; Kanaya et al., 2012; Mao et al., 2012; Griffith et al., 2013; Mallik et al., 2018), or higher than model predictions (Carslaw et al., 2001; Kubistin et al., 2010; Kim et al., 2013; Hens et al., 2014). Part of this variability may be due to interferences from alkene and aromatic based RO<sub>2</sub> radicals converting to HO<sub>2</sub> in systems that detect HO<sub>2</sub> through conversion to OH by addition of NO in the sample cell. The degree to which the RO<sub>2</sub> species can interfere with HO<sub>2</sub> measurements has been quantified through several laboratory experiments (Fuchs et al., 2011; Whalley et al., 2013; Lew et al., 2018) and estimated in some field studies (Hens et al., 2014; Crowley et al., 2018; Mallik et al., 2018). However, the extent of RO<sub>2</sub> radical contributions during HO<sub>2</sub> measurements in many of the campaigns mentioned above is unclear.

Total OH reactivity measurements can complement HO<sub>x</sub> measurements by providing a constraint on the total loss of OH that can be compared to that calculated from co-located measurements of OH sinks. Several recent studies have identified discrepancies between measured and calculated OH reactivity in which the measured values are significantly greater than the calculated values (Di Carlo et al., 2004; Hansen et al., 2014; Nölscher et al., 2016; Zannoni et al., 2016). This difference has been attributed to OH loss from unmeasured VOCs and their oxidation products. In general, significant missing OH reactivity has not been observed as often in urban environments as it has in forested areas, bringing into question our understanding of the chemistry of biogenic emissions and their oxidation products (Dusanter and Stevens, 2017).

This study reports measurements and model simulations of HO<sub>x</sub> radical chemistry as well as OH reactivity for a forested site located in Bloomington, Indiana during the 2015 IRRONIC (Indiana Radical Reactivity and Ozone productionN InterComparison) field campaign. This work compares the measured HO<sub>x</sub> radical concentrations to model predictions incorporating the Regional Atmospheric Chemistry Mechanism 2 (RACM2), in addition to a version updated to include the Leuven Isoprene Mechanism (RACM2-LIM1), as well as the Master Chemical Mechanism versions 3.2 and 3.3.1 in order to test the ability of each model to reproduce the observed radical concentrations and total OH reactivity.

## **2 Experimental section**

### **2.1 IRRONIC location and supporting measurements**

The IRRONIC campaign site was located within a mixed deciduous forest (sugar maple, sycamore, tulip polar, ash and hickory trees) at the Indiana University Research and Teaching Preserve (IU-RTP) field lab (39.1908° N, 86.502° W) located

approximately 2.5 km northeast of the center of the Indiana University campus, and 1 km from the IN 45/46 bypass at the northern perimeter. The goals of the campaign included an informal intercomparison of peroxy radical measurements by two different techniques (Kundu et al., 2019), an analysis of ozone production sensitivity at this site (Sklaveniti et al., 2018), a comparison of measured OH radical reactivity with that calculated from measured VOCs, and a comparison of measured OH, HO<sub>2</sub>, and RO<sub>2</sub> radicals with model predictions. The main biogenic emission within this area was isoprene, with an average daytime maximum mixing ratio of approximately 4 ppb during the campaign. This area exhibited low anthropogenic influence from the campus area, with an average daytime maximum mixing ratio of NO of approximately 315 ppt and an average daytime maximum NO<sub>2</sub> mixing ratio of approximately 2 ppb. Measurements were conducted on top of two scaffolding platforms adjacent to the field lab, approximately 1.8 m from the ground. Additional information regarding the field site and the IRRONIC campaign can be found in Sklaveniti et al. (2018) and Kundu et al. (2019).

Table 1 summarizes the major instrumentation employed during the campaign. NO was measured every 10 s using a chemiluminescence instrument (Thermo model 42i-TL, detection limit 50 ppt / 2 min). Periodic problems with the sensor's high voltage power supply that required an eventual replacement limited the coverage of the measurements. NO<sub>2</sub> was measured every 1 s by a Cavity Attenuated Phase Shift (CAPS) instrument (detection limit 40 ppt / 10 s), and ozone was measured every 10 sec using a 2B Technologies model 202 UV absorbance instrument (detection limit 3 ppb / 10 s). Further details on the calibration and baseline measurements for the NO, NO<sub>2</sub>, and O<sub>3</sub> measurements are described in Kundu et al. (2019). Nonmethane hydrocarbons, including C<sub>2</sub>-C<sub>10</sub> alkanes and alkenes, butadiene, C<sub>6</sub>-C<sub>9</sub> aromatic compounds, isoprene,  $\alpha$ -pinene, and  $\beta$ -pinene, were measured using a thermal desorption GC/FID instrument with a 1.5-h time resolution. Oxygenated VOCs (OVOCs), including C<sub>2</sub>-C<sub>10</sub> aldehydes, C<sub>2</sub>-C<sub>6</sub> ketones, and C<sub>2</sub>-C<sub>4</sub> alcohols, were measured by thermal desorption GC/FID-MS with a 1.5-h time resolution. Offline sampling focused on measurements of oxygenated VOCs including formaldehyde and C<sub>2</sub>-C<sub>6</sub> aldehydes, acetone, MEK, glyoxal and methylglyoxal using DNPH cartridges and HPLC-UV analysis. C<sub>6</sub>-C<sub>16</sub> VOCs including  $\alpha$ -pinene,  $\beta$ -pinene, limonene, camphene, heptane-hexadecane, methylpentene-pentadecene were measured using Sorbent cartridges and GC-MS analysis. Measurements of J(NO<sub>2</sub>) were made by spectral radiometry courtesy of the University of Houston. HONO was measured using a newly developed Laser Photofragmentation/Laser-Induced Fluorescence instrument (Bottorff et al., 2015; manuscript in preparation).

## 2.2 HO<sub>x</sub> radical measurements

The Indiana University LIF-FAGE instrument (IU-FAGE) has been described in detail previously and consists of a single axis for alternating measurements of OH and HO<sub>2</sub> or HO<sub>2</sub>\* (Dusanter et al., 2009a Griffith et al., 2013; 2016). In the LIF-FAGE technique, OH radicals are detected by laser-induced fluorescence after expansion of ambient air to low pressure. This extends the OH fluorescence lifetime, allowing temporal filtering of the fluorescence from laser scatter (Heard and Pilling, 2003). Ambient air is expanded through a 0.64 mm diameter orifice located at the top of a cylindrical nozzle (5 cm in diameter and 20 cm long), resulting in a flow rate of approximately 3 SLPM through the sampling nozzle. Two scroll pumps (Edwards XDS 35i) connected in parallel maintain a pressure inside the cell of 7.3 hPa.

The laser system used in this study consisted of a Spectra Physics Navigator II YHP40-532Q that produces approximately 8 W of radiation at 532 nm at a repetition rate of 10 kHz which is used to pump a Sirah Credo Dye laser (255 mg/L of Rhodamine 610 and 80 mg/L of Rhodamine 101 in ethanol), resulting in 40 to 100 mW of radiation at 308 nm. After exiting the dye laser, a fraction of the radiation is focused onto the entrance of a 12-m optical fiber to transmit the radiation to the sampling cell which was placed on top of the 1.8-m platform adjacent to the field lab. In the detection cell, the laser crosses the expanded air perpendicular to the flow in a White cell configuration with 24 passes. For this campaign, the laser power inside the sampling cell ranged from 0.5 to 4.4 mW and was monitored using a photodiode at the exit of the White cell.

OH radicals are excited and detected using the  $A^2\Sigma^+ v' = 0 \leftarrow X^2\Pi v'' = 0$  transition near 308 nm (Stevens et al., 1994). The net signal is measured by spectral modulation by tuning the wavelength on- and off-resonance in successive modulation cycles. A reference cell where OH is produced by thermal dissociation of water vapor is used to ensure that the laser is tuned on and off the OH transition. The OH fluorescence is detected using a microchannel plate photomultiplier tube (MCP-PMT) detector (Hamamatsu R5946U-50), a preamplifier (Stanford Research System SR445) and a gated photon counter (Stanford Research Systems SR 400). The MCP-PMT is switched off during the laser pulse through the use of electronic gating allowing the OH fluorescence to be temporally filtered from laser scattered light. A Teflon injector located approximately 2.5 cm below the inlet and 17.5 cm above the detection axis allowed for the addition of NO (approximately 2 sccm,  $1.4 \times 10^{13} \text{ cm}^{-3}$ , Matheson Gas, 10% in  $\text{N}_2$ ) to convert ambient  $\text{HO}_2$  to OH through the fast  $\text{HO}_2 + \text{NO} \rightarrow \text{OH} + \text{NO}_2$  reaction, allowing for indirect measurements of  $\text{HO}_2$ .

The IU-FAGE instrument is calibrated by producing known quantities of OH and  $\text{HO}_2$  from the photolysis of water vapor in air using a mercury penlamp within the calibration source as described previously (Dusanter et al., 2008). For these calibrations, zero air was sent through a humidifier and delivered at a flow rate of 38-50  $\text{L min}^{-1}$  to the calibration source. Uncertainties associated with the UV water photolysis calibration technique have been described previously (Dusanter et al., 2008) and are estimated to be 18% ( $1\sigma$ ) for both OH and  $\text{HO}_2$ .

### 2.2.1 Measurement of OH interferences

The LIF-FAGE measurements are subject to potential interferences where OH radicals are generated inside the detection cell. For example, ozone can be photolyzed by the laser and in the presence of water vapor can produce hydroxyl radicals (Davis et al., 1981a; 1981b) (reactions R1 and R2):



This interference in the IU-FAGE instrument is monitored through laboratory calibrations utilizing various concentrations of ozone, water vapor, and laser power. To characterize this and any other interference during ambient measurements, a chemical scrubbing technique is used to remove ambient OH prior to entering the detection cell (Griffith et al., 2016; Rickly and Stevens, 2018). This chemical modulation technique is used to monitor levels of the laser-generated ozone-water interference and any other processes that may produce OH radicals within the excitation axis.

Hexafluoropropylene (C<sub>3</sub>F<sub>6</sub>, 95.5% in N<sub>2</sub>, Matheson) is added through a circular injector 1 cm above the nozzle with a flow rate of approximately 3.5 sccm to remove 95% of externally generated OH (Rickly and Stevens, 2018). During ambient measurements, chemical addition of C<sub>3</sub>F<sub>6</sub> is modulated in between ambient OH measurements every 15 minutes for a duration of 10 minutes. The differences between the measured OH during C<sub>3</sub>F<sub>6</sub> addition and OH measurements including the interference represents the net ambient OH concentration in the atmosphere. Taking the measurement of potential interferences into account results in a limit of detection for OH for this campaign of approximately  $7.9 \times 10^5 \text{ cm}^{-3}$  for a 30 min average (S/N = 1).

### 2.2.2 Contribution of RO<sub>2</sub> interferences during HO<sub>2</sub> measurements

As discussed above, HO<sub>2</sub> radicals are measured indirectly after sampling ambient air at low pressure through chemical conversion to OH by addition of NO and subsequent detection of OH by LIF:



It was previously believed that the detection of HO<sub>2</sub> radicals using this technique was free from interferences from the reaction of RO<sub>2</sub> radicals with NO, as model simulations and measurements suggested that the rate of conversion of RO<sub>2</sub> radicals to HO<sub>2</sub> by reactions R4 and R5 and subsequent conversion to OH through reaction R3 were negligible. This was due to the slow rate of reaction R5 under the reduced oxygen concentration in the low pressure LIF-FAGE cell and the short reaction time between injection of NO and detection of OH (Heard and Pilling, 2003).



For example, RO<sub>2</sub> radicals produced from the OH-initiated oxidation of small alkanes were found to produce a negligible yield of HO<sub>2</sub> (Stevens et al., 1994; Kanaya et al., 2001; Tan, et al., 2001; Creasey et al., 2002; Holland et al., 2003). However, recent laboratory studies have shown that there are interferences associated with measurements of HO<sub>2</sub> from the conversion of RO<sub>2</sub> radicals derived from the OH-initiated oxidation of alkenes and aromatics to HO<sub>2</sub> (and subsequently OH) by reaction with NO. The high conversion efficiency of alkene-based peroxy radicals to HO<sub>2</sub> is due to the ability of the β-hydroxyalkoxy radicals produced from OH + VOC reactions to rapidly decompose, forming a hydroxyalkyl radical which then reacts rapidly with O<sub>2</sub> leading to the production of a carbonyl compound and HO<sub>2</sub> (Fuchs et al., 2011; Whalley et al., 2013; Lew et al., 2018). Because of this interference, measurements of peroxy radicals that are sensitive to this interference are denoted as HO<sub>2</sub>\* ([HO<sub>2</sub>\*] = [HO<sub>2</sub>] + α [RO<sub>2</sub>], 0 < α < 1). The conversion efficiency depends on the instrumental characteristics and configurations employed as well as the amount of NO added. The RO<sub>2</sub>-to-HO<sub>2</sub> conversion efficiencies for a number of different peroxy radicals have been characterized for current and past configurations of the IU-FAGE instrument (Lew et al., 2018). For the configuration of the IU-FAGE instrument used in this study, the conversion efficiency of isoprene-based peroxy radicals was found to be approximately 83%, while the conversion efficiency of propane peroxy radicals was found to be

approximately 15%. A high concentration of NO leading to a high conversion efficiency of isoprene-based peroxy radicals to HO<sub>2</sub> was used throughout the study to provide a useful intercomparison of the IU-FAGE HO<sub>2</sub>\* measurements with the RO<sub>2</sub>+HO<sub>2</sub> measurements by the Drexel University Ethane – Nitric Oxide Chemical Amplifier (ECHAMP) instrument (Kundu et al., 2019), as HO<sub>2</sub> and isoprene-based peroxy radicals accounted for approximately 70% of the total peroxy radicals at this site (see below). The instrumental precision for the HO<sub>2</sub>\* measurement based on the variability of the background signal due to laser scatter and detector noise results in a limit of detection for HO<sub>2</sub>\* during this campaign of  $7 \times 10^7 \text{ cm}^{-3}$  for a 30 second average (S/N = 1).

### 2.3 OH reactivity measurements

The IU Total OH Loss rate Method (TOHLM) instrument is based on the method of Kovacs and Brune (2001) and is described in detail elsewhere (Hansen et al., 2014). Briefly, the instrument is comprised of a flow tube reactor measuring 5 cm in diameter and 75 cm in length. Ambient air is introduced through an 8 cm diameter perfluoroalkoxy polymer film hose attached to the flow tube at a flow rate of approximately 180 SLPM using a regenerative blower (Spencer VB001) to establish turbulent flow conditions. Previous measurements have demonstrated that different lengths of this inlet tubing do not significantly impact the measured OH reactivity (Hansen et al., 2014). A pitot-static tube (Dwyer Instruments) is positioned just before the exit of the flow tube facing the turbulent core of the flow, approximately 1 cm from the flow tube wall. The pitot-static tube is connected to a differential pressure gauge (MKS Instruments) to measure the total flow tube velocity.

OH radicals are produced in a movable injector that houses a mercury pen lamp (UV Pen-Ray) in which the top of the pen lamp was positioned at the end of the injector, just before a spiral Teflon spray nozzle used to promote mixing within the flow tube (McMaster Carr). In addition, a turbulizer is attached to the injector tube 24 cm before the spray nozzle consisting of four 1 cm wide fins to promote turbulent flow conditions as well as to provide support of the injector throughout the flow tube. The injector is inserted along the main axis and is configured for automated movement acquiring continuous measurements in the forward and backward directions. A nitrogen flow of 10 standard liters per minute (SLPM) is bubbled through high-purity water (EMD Chemicals) producing water vapor which is directed through the injector and photolyzed by the penlamp to produce OH with typical concentrations on the order of  $10^9 \text{ cm}^{-3}$ . This method is known to also produce HO<sub>2</sub> radicals, which can lead to a regeneration of OH at NO mixing ratios greater than 1 ppbv (Kovacs and Brune, 2001). However, because the average NO mixing ratio measured over the course of the campaign was below this value, no correction to the measured reactivity was applied (Hansen et al., 2014).

OH radicals were measured using a similar FAGE detection cell described above. Ambient air was expanded through a 1 mm diameter orifice to a total pressure of approximately 8 hPa. OH radicals were excited by a portion of the 308 nm output of the dye laser, with the resulting fluorescence detected by a gated channel photomultiplier tube detector (Excelitas MP 1300) and monitored by a photon counter (Stanford Research SRS 400). A 2 meter long optical fiber was used to transmit the 308-

nm laser beam to the OH reactivity detection cell which was located inside the field lab. The laser power was measured at the exit of the detection cell and monitored with a photodiode.

As ambient air entered the flow tube, the automated OH source injector allowed for varying reaction time with the ambient air over a distance of approximately 15 cm for a period of 2.5 minutes. This produced an OH decay over a reaction time of 0-0.15 s from which the OH reactivity was determined. Losses of OH on the walls of the flow tube were measured by flowing high-purity nitrogen (Indiana Oxygen) at 180 SLPM through the flow tube in addition to the OH production through the injector to measure the decay of OH in the absence of any VOCs. Several measurements of this wall loss ( $k_b$ ) resulted in an average value of  $10 \pm 2 \text{ s}^{-1}$  ( $1\sigma$ ).

The calculated OH reactivity for a measured compound X ( $k_X$ ), can be determined from the product of the concentration of X and its second-order rate constant with OH:

$$k_X = k_{OH+X}[X] \quad (1)$$

Summation of this value for each reacting species gives the total OH reactivity ( $k_{OH}$ ):

$$k_{OH} = \sum_i k_{OH+X_i} [X_i] \quad (2)$$

Under pseudo-first order conditions ( $[OH] \ll [X]$ ), the OH concentration within the flow tube can be expressed as a first-order exponential decay:

$$[OH]_t = [OH]_0 e^{-(k_{OH}+k_b)t} \quad (3)$$

Solving for  $k_{OH}$ , the OH reactivity, gives:

$$k_{OH} = -\frac{\Delta \ln[OH]}{\Delta t} - k_b \quad (4)$$

Measurements of the change in the concentration of OH over the reaction time produces the measured OH reactivity value. These measurements can be compared to the calculated total reactivity from measured OH sinks (Eq. 2) to determine whether the measured total OH reactivity can be accounted for by the measured sinks. The difference between the measured and calculated total OH reactivity is referred to as the “missing” OH reactivity.

Laboratory measurements of the reactivity of several VOCs with well-known rate constants, including butane, isoprene, and propane showed that the OH reactivity measurements for these compounds were on average 30% lower than calculated when the measured velocity of the turbulent core is used to determine the reaction time. This consistent underestimation of the OH reactivity is likely due to either incomplete mixing of the reactants or a systematic underestimation of the reaction time (Hansen et al, 2014). As a result, the measured ambient OH reactivity values were scaled by a factor of 1.41. Measurements performed over a range of OH reactivity values suggest that the IU-TOHLM instrument can measure OH reactivity up to  $45 \text{ s}^{-1}$  with a precision ( $1\sigma$ ) of  $1.2 \text{ s}^{-1} + 4\%$  of the measured value for a 10 min average (Hansen et al., 2014).



## 2.4 Modeling HO<sub>x</sub> concentrations and OH reactivity

Ambient measurements of OH, HO<sub>2</sub><sup>\*</sup>, and total OH reactivity were modeled with the Regional Atmospheric Chemistry Mechanism (RACM2) (Goliff et al., 2013) and the Master Chemical Mechanism version 3.2 (Jenkin et al., 1997; Saunders et al., 2003). While the MCM model provides a near-explicit chemical mechanism and is expected to better represent complex chemical atmospheres, the lumped RACM mechanism is easier to use in radical budget calculations. The isoprene oxidation mechanism in RACM2 was updated as described in Tan et al. (2017) to include the Leuven Isoprene Mechanism (LIM1) originally proposed by Peeters, et al. (2009) involving peroxy radical isomerization reactions leading to additional HO<sub>x</sub> radical production, and includes the LIM1 updated bulk RO<sub>2</sub> reactions described in Peeters et al. (2014). The addition also includes a revision of the chemistry of first-generation isoprene oxidation products, including methyl vinyl ketone (MVK), methacrolein (MACR), and isoprene hydroperoxides (ISHP) (Tan et al., 2017). In addition, the ambient measurements were also modeled with version 3.3.1 of the Master Chemical Mechanism (MCM). In comparison to MCM 3.2, MCM 3.3.1 includes an updated isoprene oxidation mechanism based on the LIM1 mechanism resulting in HO<sub>x</sub> recycling from peroxy radical H-shift isomerization reactions (Jenkin et al., 2015).

The Framework for 0-D Atmospheric Modeling (F0AM) was used to calculate the radical concentrations and OH reactivity observed at the IRRONIC site (Wolfe et al., 2016). The model was constrained by the 30 minute average measured mixing ratios of ozone, NO<sub>x</sub>, and VOCs and processed through a 5 day spin-up to generate unmeasured secondary oxidation products. Table S1 summarizes the measured compounds and includes their grouping into the condensed RACM2 model inputs. Because the VOC measurements occurred every 90 minutes, the measurements were interpolated into 30 min bins before input to the model. Due to the minimal overlap of the NO measurements with the HO<sub>x</sub> measurements, the model was constrained to the measured diurnal averaged mixing ratio of NO for all days. Zero-dimensional models cannot explicitly account for emissions, and NO is emitted both by vehicles on the nearby highway 1 km to the Southwest and by soil. Such local perturbations to the NO<sub>x</sub>-O<sub>3</sub>-radical chemistry necessitate using constrained measurements of NO, NO<sub>2</sub>, and O<sub>3</sub>. The measured J(NO<sub>2</sub>) was used to scale the model calculated J(NO<sub>2</sub>) and other photolysis rates. The model uncertainty is approximately 30% (1σ), estimated from uncertainties associated with the input parameters and the rate constants for each reaction (Griffith et al., 2013; Wolfe et al., 2016).

## 3 Results and discussion

Campaign diurnal average measurements of J(NO<sub>2</sub>), temperature, isoprene, O<sub>3</sub>, NO<sub>2</sub>, and NO are summarized in Fig. 1. The maximum average mixing ratio of NO of approximately 315 ppt was observed at approximately 08:00 (EDT), while the average mixing ratio of NO<sub>2</sub> reached a maximum of 2 ppb around 10:00. Average mixing ratios of isoprene ranged from 0.4 to 4.4 ppb, reaching a maximum around 18:00. Anthropogenic VOCs were relatively low at this site, with maximum mixing ratios of benzene less than 80 ppt. Day-to-day profiles (July 10 to July 25) are illustrated in Fig. 2, showing measurements of

O<sub>3</sub>, temperature, isoprene, NO<sub>x</sub>, HO<sub>2</sub><sup>\*</sup>, and OH. Unfortunately, instrumental problems limited the NO measurements prior to 19 July.

### 3.1 OH measurements and model comparison

OH concentrations were determined using the chemical modulation technique described above using external C<sub>3</sub>F<sub>6</sub> addition to scavenge ambient OH and measure interferences producing OH inside the IU-FAGE detection cell, including laser generated OH. The measured interferences were subtracted from the total OH signal determined from spectral modulation, resulting in net ambient OH concentrations (Fig. 2). As can be seen from this figure, the measured interference was a significant fraction of the total OH signal on many days.

Figure 3 illustrates the total measured OH radical signal by spectral modulation (black circles), the measured interference (blue squares), and the expected laser-generated interference from reactions 3 and 4 calculated from laboratory calibrations (Griffith et al., 2016) (green points) during 14 July and 15 July. On 15 July, the measured interference was similar to the calculated interference suggesting that the majority of the measured interference was laser-generated. However, on 14 July, the measured interference was much larger than the calculated interference, suggesting that the majority of the measured interference was due to an unknown source. Subtraction of the calculated laser-generated interference from the measured interference on all days resulted in a measurement of the unknown interference that increased with both ozone and temperature during the campaign (Fig. 4).

This result is consistent with the observations from Mao et al. (2012) who found that the interference measured in their LIF-FAGE instrument using a similar chemical modulation technique increased with ozone and total OH reactivity. The observed increase in the magnitude of the unknown interference with ozone and temperature suggests that the interference may be related to the ozonolysis of biogenic VOCs, whose emissions increase with temperature. This result is also consistent with the measurements of Novelli et al. (2017), who found that their observed interference correlated with the product of ozone and biogenic VOC concentrations, although the correlation in the present study was not statistically significant. Previous measurements have shown that some LIF-FAGE instruments, including the IU-FAGE instrument, are susceptible to an interference under high concentrations of ozone and biogenic VOCs, perhaps due to the decomposition of Criegee intermediates inside the FAGE detection cell (Novelli et al., 2014; Fuchs et al., 2016; Novelli et al., 2017; Rickly and Stevens, 2018). However, estimated concentrations of Criegee intermediates in similar environments on the order of  $5 \times 10^4 \text{ cm}^{-3}$  (Novelli et al., 2017) are too low to explain the observed interference during the IRRONIC campaign.

The observation of a significant interference during this campaign is in contrast to previous measurements of OH by the IU-FAGE instrument in a forested environment during the CABINEX 2009 campaign (Griffith et al., 2013). During this campaign, several tests were conducted where C<sub>3</sub>F<sub>6</sub> or CO was added to remove ambient OH. These tests did not reveal any significant interference, and measurements of OH were found to be in good agreement with model predictions (Griffith et al., 2013). One possible explanation for this discrepancy with the measurements during IRRONIC is the lower levels of ozone and temperatures observed during CABINEX compared to IRRONIC. Average mixing ratios of ozone during CABINEX were

near 30 ppb and average temperatures were near 20°C during the day, with average mixing ratios of isoprene less than 2 ppb in the afternoon. These levels of ozone and temperature are lower than that where the interference was observed during IRRONIC (Fig. 4), suggesting that a similar interference was likely undetectable during CABINEX.

Recent measurements have found that NO<sub>3</sub> radicals can lead to an interference in FAGE instruments (Fuchs et al., 2016), although the mechanism for production of this interference is not known. Such an interference in the IU-FAGE instrument could explain the observed interference during some nights (Fig. 3), but is unlikely the source of the interference during the daytime. Another possible source of the interference is the decomposition of ROOOH molecules inside the FAGE detection cell formed from the reaction of OH with RO<sub>2</sub> radicals (Fittschen et al., 2019). However, assuming a rate constant of  $1 \times 10^{-10} \text{ cm}^3 \text{ s}^{-1}$  for the OH + RO<sub>2</sub> reaction, it is unlikely that a significant fraction of RO<sub>2</sub> radicals will react to form ROOOH under the mixing ratios of NO observed at this site, as the estimated lifetime of RO<sub>2</sub> radicals with respect to reaction with NO was an order-of-magnitude shorter than that for reaction with OH. Additional measurements and laboratory tests will be needed to identify and minimize interferences associated with LIF-FAGE measurements of OH.

The day-to-day measurements of OH after the interference has been subtracted for 10-20 July and 24-25 July are illustrated in Fig. 5. Measurements on 21-22 July focused on measurements of HO<sub>2</sub>\* as part of the peroxy radical informal instrumental intercomparison (Kundu et al., 2019), with NO added continuously to the detection cell to provide measurements with a higher time resolution. Thus OH measurements were not conducted on these days. This figure also illustrates the day-to-day model results for OH and HO<sub>2</sub>\* from the MCM models 3.2 and 3.3.1 and the base RACM2 and the modified RACM2-LIM1 models, illustrating that, the predicted OH concentrations are generally lower than the measured concentrations.

Figure 6 (top) shows the average diurnal profile of the 15-min OH measurements, both with and without the measured interference, binned into 1 hour time periods for the days illustrated in Fig. 5. The average ambient diurnal OH radical concentration reached a maximum of approximately  $4\text{-}5 \times 10^6 \text{ cm}^{-3}$  after the measured interference was subtracted. If the measured interference was not subtracted from the total OH signal determined by spectral modulation, the resulting OH radical concentrations would be as high as  $9 \times 10^6 \text{ cm}^{-3}$  (Fig. 6), much greater than the MCM and RACM2 modeled diurnal average maximum concentrations of approximately  $2 \times 10^6 \text{ cm}^{-3}$ . The daytime OH radical concentration measurements after the interference has been subtracted are in better agreement with the model results, but are still approximately a factor of two larger from 12:00 to midnight and appear to peak later than the model predictions. Including versions of the LIM1 mechanism for HO<sub>x</sub> regeneration in both the MCM (3.3.1) and RACM2 (RACM2-LIM1) models result in somewhat higher modeled daytime concentrations of OH compared to the base MCM 3.2 and RACM2 mechanisms, although the results are still lower than the measured concentrations (Fig. 6).

A possible reason for the model underprediction of the measurements is an underestimation of the concentration of NO in the model. As discussed above, instrumental problems limited the measurements of NO primarily to several days at the end of the campaign, resulting in approximately 2-3 days that overlapped with the OH measurements (Fig. 2). Consistent measurements were only obtained after replacing the instrument's detector. In order to model the remaining days of the campaign, the model was constrained to the diurnal average of the NO measurements from the latter half of the campaign.

1 However, it is possible that the actual mixing ratio of NO during the early days of the campaign was higher than the average  
2 value measured during the end of the campaign, given that the measured NO<sub>2</sub> concentrations during the early part of the  
3 campaign were approximately a factor of 2 greater than that measured during the latter part of the campaign (20-24 July) (Fig.  
4 2). For the days at the end of the campaign where there was significant overlap between the measurements of OH and NO, the  
5 model results are in better agreement during these days (20 and 24 July) (Fig. 5). On 20 July, the RACM2-LIM1 and MCM  
6 3.3.1 models predict maximum OH concentrations that are within 30% of the measured OH on 20 July (Fig. S1).

7 The diurnal average model results are in better agreement with the measurements when mixing ratios of NO were  
8 unconstrained while constraining mixing ratios of NO<sub>2</sub> and O<sub>3</sub>. As shown in Fig. 6, unconstraining the concentration of NO in  
9 the MCM models increases the predicted OH concentrations by approximately a factor of 3 during the daytime with model  
10 predicted mixing ratios of NO approximately a factor of 2 greater than the constrained values during the day. Similar results  
11 were found when NO was unconstrained in the RACM2 models (Fig. S2). However, the assumption that NO is in steady-state  
12 may not be justified given the location of the site near NO sources from transportation as well as the potential influence of soil  
13 emissions (Molina-Herrera et al., 2017). In addition, the measurements suggest that deviations from the ozone photostationary  
14 state were significant at this site, implying that the concentrations of peroxy radicals were high enough to significantly impact  
15 the concentration of NO. On the days when NO was measured, the models overpredicted the NO measurements by a factor of  
16 approximately 2-4 during the day, and underpredicted the measurements in the morning and evening (Fig. S3). This  
17 underprediction of the measured NO in the morning and evening may reflect active NO sources from soil and transportation  
18 emissions, and could explain why the NO unconstrained model underpredicts the concentration of OH in the afternoon.  
19 Although the model still underestimates the measurements of OH, it is clear that without taking the observed OH interference  
20 into account, the measured OH concentrations would have been a factor of 5 greater than predicted by the model mechanisms,  
21 similar to previous measurements under comparable mixing ratios of isoprene and NO<sub>x</sub> (Rohrer et al., 2014).

## 22 **3.2 HO<sub>2</sub>\* measurements and model comparison**

23 The day-to-day measurements of HO<sub>2</sub>\* are illustrated in Fig. 5 with the MCM 3.2, MCM 3.3.1, RACM2, and RACM2-LIM1,  
24 model results. The contribution of modeled RO<sub>2</sub> radicals to the modeled HO<sub>2</sub>\* is based on laboratory calibrations of the RO<sub>2</sub>-  
25 to-HO<sub>2</sub> conversion efficiencies for the sampling conditions used in this study (Lew et al., 2018) and are incorporated into both  
26 versions of the RACM2, and MCM peroxy radical categories. Under the instrumental conditions during the campaign, the  
27 conversion efficiency of isoprene-based peroxy radicals to HO<sub>2</sub> was determined to be approximately 83 ± 7%, while the  
28 conversion efficiency of methyl peroxy radicals was estimated to be approximately 5% (Lew et al., 2018). These two peroxy  
29 radicals accounted for the majority of RO<sub>2</sub> radicals predicted by the models (see below). The maximum measured HO<sub>2</sub>\*  
30 concentration each day during the campaign was generally between approximately 2 × 10<sup>8</sup> and 2 × 10<sup>9</sup> molecules cm<sup>-3</sup> (Figs.  
31 2 and 5), with an average daily maximum value of approximately 1 × 10<sup>9</sup> cm<sup>-3</sup> (Fig. 6). The RACM2-LIM1 and MCM 3.3.1  
32 modeled diurnal averaged HO<sub>2</sub>\* reached a maximum of approximately 1.4 × 10<sup>9</sup> cm<sup>-3</sup> and 1.3 × 10<sup>9</sup> cm<sup>-3</sup>, respectively,  
33 compared to a value of 1.2 × 10<sup>9</sup> cm<sup>-3</sup> for the RACM2 and MCM 3.2 modeled HO<sub>2</sub>\* (Fig. 6).

The predicted HO<sub>2</sub>\* concentrations by the base RACM2 model are in good agreement with the measured concentrations, overpredicting the measurements by approximately 20% on average, although the model agrees with the measurements to within the combined uncertainty of the model and the measurements. Including the LIM1 mechanism in the RACM2 mechanism increases the modeled HO<sub>2</sub>\* by approximately 15% due to the modeled increase in HO<sub>x</sub> radical production from the isomerization of isoprene-based peroxy radicals. These results are in contrast to that observed during the CABINEX campaign, where a RACM-based model overpredicted the measured HO<sub>2</sub>\* by as much as a factor of 2 (Griffith et al., 2013), likely related to the higher concentrations of NO observed during IRRONIC compared to CABINEX increasing the importance of the HO<sub>2</sub> + NO and RO<sub>2</sub> + NO reactions in determining the fate of these radicals.

The MCM-based model results are also in good agreement with the measured HO<sub>2</sub>\*, also overpredicting the measured concentrations by approximately 20% on average in the afternoon (Fig. 5 and 6). The MCM 3.3.1 mechanism results in predicted HO<sub>2</sub>\* concentrations that are approximately 5% greater than that predicted by MCM 3.2 in the afternoon when NO concentrations are low due to the inclusion of HO<sub>x</sub> production from the isomerization of isoprene-based peroxy radicals. These results are also consistent with a possible underestimation of the actual concentrations of NO at the site as discussed above. Unconstraining the mixing ratio of NO in the MCM models increase the averaged modeled HO<sub>2</sub>\* concentrations by approximately 10%, but they are still within the combined uncertainty of the model and the measurements (Fig. 6). Similar results were found when NO was unconstrained in the RACM2 models, although the higher daytime NO predicted by these models resulted in lower daytime HO<sub>2</sub>\* concentrations when compared to the NO constrained models, while the lower predicted nighttime NO resulted in predicted HO<sub>2</sub>\* concentrations by the base RACM2 model that were significantly greater compared to both the NO constrained model results and the measurements (Fig. S2).

The MCM 3.2 and MCM 3.3.1 diurnal average modeled HO<sub>2</sub>\* concentrations and the model contribution of peroxy radicals to HO<sub>2</sub>\* are shown in Fig. 7 (left panels). The diurnal profile of the HO<sub>2</sub>\* radical concentration predicted by the MCM models includes contributions primarily from isoprene peroxy radicals and HO<sub>2</sub> radicals, with smaller contributions from methyl peroxy and acetyl peroxy radicals (Fig. 7). The RACM2 models produced similar results, with HO<sub>2</sub> and isoprene peroxy radicals contributing to the majority of the modeled HO<sub>2</sub>\* concentrations (Fig. S4). The total modeled RO<sub>x</sub> (RO<sub>2</sub> + HO<sub>2</sub>) concentrations by the different mechanisms are also shown in Fig. 7 (right panels). The MCM 3.2 model predicted that the diurnal average total RO<sub>x</sub> concentration consisted primarily of HO<sub>2</sub> (52%), isoprene peroxy radicals (20%), methyl peroxy (CH<sub>3</sub>O<sub>2</sub>, 22%), and acetyl peroxy (CH<sub>3</sub>CO<sub>3</sub>, 5%), with daytime (08:00 – 20:00) contributions of 48%, 26%, 19%, and 5% for HO<sub>2</sub>, isoprene peroxy, CH<sub>3</sub>O<sub>2</sub>, and CH<sub>3</sub>CO<sub>3</sub>, respectively. The MCM 3.3.1 model predicted that HO<sub>2</sub> (53%), isoprene peroxy (16%), methyl peroxy (23%), acetyl peroxy (5%) were the major contributors to the modeled diurnal average total RO<sub>x</sub> concentration, with daytime contributions of 50%, 22%, 21%, and 6% (Fig. 7). Similar results were obtained from the RACM2 models (Fig. S4). As discussed above, the configuration of the IU-FAGE instrument used in this study converted approximately 83% of isoprene peroxy radicals to HO<sub>2</sub> upon addition of NO and minimally converts methyl peroxy radicals to HO<sub>2</sub> (<5%) (Lew et al., 2018). Thus, the majority of the contributing species to the measured HO<sub>2</sub>\* are HO<sub>2</sub> and isoprene peroxy radicals which together account for approximately 70% of the total peroxy radical concentration predicted by these models.

Measurements of the total HO<sub>2</sub> + RO<sub>2</sub> radical concentrations using an Ethane – Nitric Oxide Chemical Amplifier (ECHAMP) were found to be in good agreement with the HO<sub>2</sub>\* measurements reported here and are summarized in Kundu et al. (2019).

### 3.3 Total OH reactivity measurements and model comparison

The measured total OH reactivity and that calculated from measured OH sinks using both the RACM and MCM mechanisms are shown in Fig. 8, where the measured OH reactivity is averaged into 2 hour bins. As illustrated in this figure, the calculated OH reactivity was in relatively good agreement with the measured OH reactivity on some days and nights, specifically 15-16 July, with missing reactivity observed later in the campaign. Overall, the averaged measured OH reactivity varied between the instrumental limit of detection of 1 s<sup>-1</sup> to a maximum of approximately 31 s<sup>-1</sup> with an overall diurnal average value of approximately 13 s<sup>-1</sup>.

The campaign diurnal averaged measured OH reactivity is shown in Fig. 9 along with the calculated total OH reactivity from the measured OH sinks. On average, the calculated reactivity is in good agreement with the measurements. As expected for this deciduous forest environment, isoprene was the dominant contributor making up 37% of the diurnally averaged total reactivity, followed by OVOCs (28%), inorganics (10%), alkanes and alkenes (5%), anthropogenic non-methane hydrocarbons (NMHC) (1%), and monoterpenes (<1%) with missing reactivity accounting for the remaining 18% (Fig. S5). During the daytime (08:00 and 20:00) the contributions are similar, with isoprene being the largest contributor at 47% followed by OVOCs (24%), inorganics (8%), alkanes and alkenes (4%), anthropogenic NMHC (1%), and monoterpenes (<1%) with missing reactivity accounting for the remaining 14%. During the nighttime, (20:00 to 08:00), OVOCs were the dominant contributor to the modeled OH reactivity at 32% followed by isoprene (24%), inorganics (11%), alkanes and alkenes (6%), anthropogenic NMHC (2%), and monoterpenes (<1%) with missing reactivity of 24% (Fig. S5).

The campaign diurnal average (Fig. 9) shows a correlation with temperature, with the maximum average OH reactivity of approximately 20 s<sup>-1</sup> occurring around 13:30. The calculated reactivity was consistent with the measured reactivity for temperatures less than 294 K, while the observed reactivity is greater than that calculated from the measured sinks for higher temperatures, although at temperatures above 302 K the measured reactivity appears to be less than calculated (Fig. S6). These results are similar to that reported by Hansen et al. (2014) and Di Carlo et al. (2004) in which the measured missing reactivity appeared to increase with temperature.

Figure 9 also shows the campaign average OH reactivity including the reactivity of unmeasured oxidation products predicted by the MCM 3.3.1 model. On average, including the contribution of unmeasured oxidation products can account for the majority of the missing reactivity. While the model tends to overpredict the average measured reactivity in the afternoon and evening, the model results agree to within the combined uncertainty of the model and the precision of the measurement (Hansen et al., 2014). Similar results were obtained by the RACM2 models, although the predicted reactivity of unmeasured oxidation products by the RACM2 models are approximately a factor of two smaller than that predicted by the MCM models (Fig. S7). These results suggest that the models are generally able to reproduce the measured OH reactivity at this site, and

that the missing reactivity observed during IRRONIC may be due to unmeasured oxidation products, with isoprene nitrates and isoprene epoxides within the RACM2 and MCM mechanisms being the primary contributors to the missing reactivity.

While the campaign averaged OH reactivity measurements appear to be in reasonable agreement with the calculated reactivity based on measured compounds, there were several days that displayed large missing reactivity similar to that observed by Hansen et al. (2014). The MCM 3.3.1 model results for a day with the largest missing reactivity (17 July) is shown in Fig. 10, indicating that the modeled reactivity including unmeasured oxidation products cannot explain the observed reactivity on this day. The reason for this discrepancy is unclear, as the missing reactivity on this day did not appear to correlate with changes in wind speed, direction, trajectory, or meteorological conditions, but may indicate the presence of additional unmeasured emissions or oxidation products not accounted for by the model. Additional measurements and analyses will be necessary to determine the source of the missing reactivity.

### 3.4 Radical budgets

The analysis of the rates of radical initiation, propagation, and termination can provide insight to the importance of individual radical sources and sinks. For the IRRONIC campaign, the OH radical budget is illustrated in Fig. 11, where OH radical production reactions are represented in shades of blue and loss reactions are represented in shades of red. Daytime production includes reactions with both initiation and propagation that produces OH radicals (positive rates), while daytime OH loss reactions are represented by propagation and termination reactions that remove OH (negative rates). For simplicity only the RACM2 and RACM2-LIM1 radical budgets are shown.

The maximum rates for the OH radical budget of approximately  $2.7 \times 10^7 \text{ cm}^3 \text{ s}^{-1}$  from the RACM2-LIM1 model were higher than the maximum value of  $2.2 \times 10^7 \text{ cm}^3 \text{ s}^{-1}$  in RACM2. The addition of the LIM1 mechanism increases the OH radical production rate mostly from photolysis of hydroxypetroxy aldehydes (HPALD) produced from the isomerization of isoprene-based peroxy radicals and their subsequent chemistry (Peeters et al., 2014; Tan et al., 2017). In the RACM2-LIM1 model, the daytime OH radical production is dominated by the  $\text{HO}_2 + \text{NO}$  reaction from 10:00 to 14:00 (59%) and drops to 29% from 14:00 to 18:00. Ozone photolysis and the LIM1 mechanism contribute up to 31% and 20% of the total OH radical production from 14:00 to 18:00, with ozonolysis ( $\text{VOC} + \text{O}_3$ ) and photolysis of HONO,  $\text{H}_2\text{O}_2$ , methacrolein (MACR), and organic peroxides (OP1, OP2) contributing to 8% and 10% of the total OH radical production in the afternoon (Fig. 11). A majority of the OH radical loss is due to OH reactions with VOCs (63-68%) and OVOCs (29-26%) during the morning and afternoon. As described above, the measured total OH reactivity was in reasonable agreement with the modeled OH reactivity; therefore, it is likely that the total OH loss is well represented in the model. An experimental radical budget for 20 July when the measurements were complete suggests that the total measured OH production rate is nearly balanced by the total OH loss rate calculated by the concentration of individual sinks and the loss rate based on the measured total OH reactivity to within approximately 30% (Fig. S8), consistent with the agreement between the measured and modeled OH on this day as discussed above. For simplicity, the measured  $\text{HO}_2^*$  was used to calculate the rate of OH production from the  $\text{HO}_2 + \text{NO}$  reaction and as a result the measured production rate represents an upper limit to the overall OH production rate. Thus, the difference

1 between production and loss may be greater than illustrated in this figure, but is still likely to be within the combined  
2 uncertainties of all the measurements (38% ( $2\sigma$ ) for OH and for  $\text{HO}_2^*$  for example), similar to that observed previously (Tan  
3 et al., 2019).

4 The total radical ( $\text{RO}_x$ ) budget from the RACM2 mechanisms of OH,  $\text{HO}_2$ , and  $\text{RO}_2$  radicals is illustrated in Fig. 12.  
5 Overall, total radical initiation in the RACM2-LIM1 mechanism was larger, with a maximum value of approximately  $3.2 \times$   
6  $10^7 \text{ cm}^{-3} \text{ s}^{-1}$  compared to RACM2 maximum value of approximately  $2.2 \times 10^7 \text{ cm}^{-3} \text{ s}^{-1}$ . The increase in total radical initiation  
7 in the RACM2-LIM1 model is due to both the added radical initiation from the photolysis of HPALDs as well as increased  
8 radical initiation from other aldehydes produced in the LIM1 mechanism. Overall, radical initiation from the photolysis of  
9 HPALDs and the subsequent chemistry from the LIM1 mechanism contributed 16-22% of total radical initiation during the  
10 day, while photolysis of formaldehyde and other aldehydes contributed to approximately 42% of total radical initiation, with  
11 ozone photolysis contributing to 29-33% of radical initiation in the mornings and afternoon (Fig. 12). In contrast, ozone  
12 photolysis contributes to approximately 43% of radical initiation in the RACM2 mechanism compared to formaldehyde and  
13 other aldehydes contributing 22-24% (Fig. 12). Radical termination for both mechanisms is dominated by peroxy radical self-  
14 reactions, such as the  $\text{HO}_2 + \text{HO}_2$  reaction, as well as the reaction of  $\text{HO}_2$  with isoprene-based peroxy radicals (ISOP) and  
15 other peroxy radicals ( $\text{RO}_2$ ). These reactions account for approximately 80% of radical termination due to the low levels of  
16  $\text{NO}_x$  used in the models, with reaction of OH +  $\text{NO}_2$  and other  $\text{NO}_x$  radical reactions accounting for approximately 20% of  
17 radical termination in these models (Fig. 12). As discussed above, it is possible that the NO concentration used to constrain  
18 the model may be lower than the actual concentration. As a result, the modeled contribution of  $\text{NO}_x$  reactions to radical  
19 termination may represent a lower limit to the actual contribution.

20 The partitioning of the total radical budget production for IRRONIC is similar to the modeled budget observed during  
21 PROPHET 2008 and CABINEX 2009 (Griffith et al., 2013). The updated RACM model used during these campaigns predicted  
22 that radical termination was dominated by  $\text{HO}_2 + \text{RO}_2$  reactions (including the  $\text{HO}_2 + \text{ISOP}$  reaction), contributing to  
23 approximately 80% of total radical termination, similar to the 74% for the  $\text{HO}_2 + \text{ISOP}$  and  $\text{HO}_2 + \text{RO}_2$  reactions predicted here  
24 by the RACM2 model. The photolysis of ozone accounted for approximately 20-30% of total radical initiation during these  
25 campaigns based on an updated version of the RACM model (Griffith et al., 2013) compared to approximately 40% predicted  
26 by the RACM2 mechanism during IRRONIC due to higher concentrations observed during this campaign. Ozonolysis  
27 reactions contributed to approximately 20-30% of total radical initiation during PROPHET and CABINEX compared to 10-  
28 11% during IRRONIC. Photolysis of HCHO and other aldehydes contributed to approximately 22-24% of the total rate of  
29 radical initiation during IRRONIC compared to 23% and 5% during PROPHET 2008 and CABINEX 2009, respectively, with  
30 the low contribution during CABINEX primarily due to the lower mixing ratios of HCHO observed during this campaign  
31 (Griffith et al., 2013). In contrast, photolysis of HONO was a significant radical source during PROPHET and CABINEX,  
32 contributing 14-17% of radical initiation compared to approximately 3% of total radical production during IRRONIC due to  
33 the lower mixing ratios of HONO observed during IRRONIC. On average, mixing ratios of HONO during IRRONIC were  
34 approximately 40 ppt at night decreasing to approximately 10 ppt during the day (Fig. S9) compared to daytime mixing ratios



between 50 and 75 ppt during PROPHET and CABINEX (Griffith et al., 2013). The reason for the difference in the measured HONO values between these two sites is unclear, but may be related to increased production from photolysis of nitric acid on the forest canopy surfaces at the PROPHET site (Zhou et al., 2011).

## 4 Summary

Measurements of OH radical concentrations using the IU-FAGE instrument during the IRRONIC campaign revealed a significant unknown interference that appeared to correlate with both temperature and ozone. The average measured OH radical concentration after the interference was subtracted reached an average daytime maximum of approximately  $4\text{--}5 \times 10^6 \text{ cm}^{-3}$ . This is in contrast to the measurements including the interference which reached an average daytime maximum of approximately  $9 \times 10^6 \text{ cm}^{-3}$ . Similar concentrations of OH were observed at this site in 2017 during an informal intercomparison between the IU-FAGE instrument and the University of Colorado Chemical Ionization Mass Spectrometry (CIMS) instrument (Rosales et al., 2018; Reidy et al., 2018).

After subtracting the interference, the OH measurements were in better agreement with model simulations utilizing the Regional Atmospheric Chemical Mechanism 2 (RACM2) with an updated Leuven Isoprene Mechanism (LIM1) as well as the Master Chemical Mechanism versions 3.2 and 3.3.1. Both the RACM2-LIM1 and MCM 3.3.1 mechanisms add radical recycling reactions for isoprene oxidation that increase the modeled OH and peroxy radical concentrations. The addition of radical recycling by isoprene still resulted in model predictions of OH that were approximately a factor of two lower than the measured concentrations. One possible explanation for the discrepancy is an underestimation of the mixing ratio of NO during the campaign, as instrumental difficulties prevented measurements of NO except at the end of the campaign. Unconstraining the mixing ratio of NO in the model while constraining NO<sub>2</sub> and O<sub>3</sub> to their measured values leads to an increase in the modeled mixing ratios of NO resulting in an increase in the average modeled OH concentration by approximately a factor of 2-3, improving the agreement with the measured OH concentrations. These higher values of NO<sub>x</sub> are comparable to that observed at this site in 2017 when measured OH concentrations were similar to that observed here (Rosales et al., 2018; Reidy et al., 2018). However, it is clear that if the measured interference was not taken into account, the apparent OH concentrations would have been a factor of 5 greater than predicted by the model mechanisms, comparable to previous measurements under low NO<sub>x</sub> and high isoprene conditions (Rhorer et al., 2014). These results are similar to that reported by Mao et al. (2012) and Mallik et al. (2017) who found good agreement between their OH measurements and model predictions when measured interferences were taken into account. However, because of differences in instrument design (geometry, cell pressure, flow, etc.) these interferences may not significantly impact other LIF-FAGE instruments. However, future OH measurements using the LIF-FAGE technique should include methods to quantify potential instrumental artifacts even if they are insignificant, to demonstrate that the measurements are free from interferences.

Measurements of total OH reactivity were in reasonable agreement with that calculated from measured OH sinks, with isoprene contributing approximately 37% and OVOCs 28% of the diurnally averaged measured reactivity, with 18% of

1 the measured reactivity missing. However, on average the missing reactivity fraction can be explained by unmeasured  
2 oxidation products, specifically from isoprene nitrates and isoprene epoxides within the RACM2 and MCM mechanisms. This  
3 indicates that these mechanisms are accurately representing the total OH loss at this site.

4 Measurements of HO<sub>2</sub> radicals by the IU-FAGE instrument using chemical conversion to OH by addition of NO has  
5 been shown to be sensitive to alkene-based peroxy radicals (Lew et al., 2018). As a result, the measurements represent a sum  
6 of HO<sub>2</sub> and a fraction of RO<sub>2</sub> radicals in the atmosphere (HO<sub>2</sub>\*). During the IRRONIC campaign, the measured HO<sub>2</sub>\*  
7 concentration primarily reflected the sum of HO<sub>2</sub> and isoprene-based peroxy radicals, which contributed to approximately 70%  
8 of the total modeled peroxy radicals. The average daytime ambient HO<sub>2</sub>\* measurements reached maximum concentrations of  
9 approximately  $1 \times 10^9 \text{ cm}^{-3}$ . Both MCM models predicted HO<sub>2</sub>\* concentrations that were in good agreement with the  
10 measurements, while the RACM mechanisms resulting in predicted concentrations that were approximately 20-35% greater  
11 than the measurements but within the combined uncertainty of both the model and the measurement. These results are also  
12 consistent with an underestimation of the NO concentrations in the model, as increasing the modeled NO resulted in modeled  
13 HO<sub>2</sub>\* concentrations that were still in good agreement with the measurements. These results are in contrast to some previous  
14 measurements in forest environments where model predictions were found to be significantly greater than measured HO<sub>2</sub>\*  
15 concentrations (Griffith et al., 2013), perhaps as a result of the lower mixing ratios of NO observed at these sites. Additional  
16 measurements are needed in order to resolve this discrepancy, which may be related to a gap in our understanding of peroxy  
17 radical chemistry under low NO conditions.

**Data availability.** Data are available upon request from the corresponding author ([pstevens@indiana.edu](mailto:pstevens@indiana.edu)).

**Competing interests.** The authors declare that they have no conflicts of interest.

**Author contributions.** PS, SD and EW designed the research project. ML, PR, BB, and PS were responsible for the LIF-  
FAGE OH, HO<sub>2</sub>\*, OH reactivity, and HONO measurements. SK and EW were responsible for the supporting measurements  
of NO, NO<sub>2</sub>, and O<sub>3</sub>. SD, SS, TL, and NL were responsible for the measurements of VOCs and OVOCs. ML, PR, ER, and PS  
conducted the analysis and photochemical modelling and wrote the paper with feedback from all co-authors. ML and PR  
contributed equally to the paper.

**Acknowledgements.** This study was supported by the National Science Foundation, grant AGS-1440834 to Indiana  
University, AGS-1443842 to the University of Massachusetts, and AGS-1719918 to Drexel University. This work was also  
supported by grants from the Regional Council Nord-Pas-de-Calais through the MESFOZAT project, the French National  
Research Agency (ANR-11-LABX-0005-01) and the European Regional Development Fund (ERDF) through the CaPPA  
(Chemical and Physical Properties of the Atmosphere) project, and the Région Hauts-de-France, the Ministère de

l'Enseignement Supérieur et de la Recherche and ERDF through the CLIMIBIO project. We would like to thank J. Flynn (University of Houston) for the spectroradiometer used to obtain the  $J(\text{NO}_2)$  measurements.

## References

- Ait-Helal, W., Borbon, A., Sauvage, S., de Gouw, J. A., Colomb, A., Gros, V., Freutel, F., Crippa, M., Afif, C., Baltensperger, U., Beekmann, M., Doussin, J.-F., Durand-Jolibois, R., Fronval, I., Grand, N., Leonardis, T., Lopez, M., Michoud, V., Miet, K., Perrier, S., Prévôt, A. S. H., Schneider, J., Siour, G., Zapf, P., and Locoge, N.: Volatile and intermediate volatility organic compounds in suburban Paris: variability, origin and importance for SOA formation, *Atmos. Chem. Phys.*, 14, 10439–10464, 2014
- Badol, C., Borbon, A., Locoge, N., Leonardis, T., and Galloo, J. C.: An automated monitoring system for VOC ozone precursors in ambient air: development, implementation and data analysis, *Anal. Bioanal. Chem.*, 378, 7, 1815–1827, 2004.
- Bottorff, B., Stevens, P. S., Lew, M., Rickly, P., and Dusanter, S. Measurements of Nitrous Acid (HONO) in an Indiana Forest by Laser Photofragmentation/Laser-Induced Fluorescence (LP/LIF), Abstract A21B-0116 presented at 2015 Fall Meeting, AGU, San Francisco, CA, 14-18 Dec., 2015.
- Carslaw, N., Creasey, D. J., Harrison, D., Heard, D. E., Hunter, M. C., Jacobs, P. J., Jenkin, M. E., Lee, J. D., Lewis, A. C., Pilling, M. J., Saunders, S. M., and Seakins, P. W.: OH and HO<sub>2</sub> Radical Chemistry in a Forested Region of North-Western Greece, *Atmos. Environ.*, 35, 4725–4737, 2001.
- Chen, S., Ren, X., Mao, J., Chen, Z., Brune, W. H., Lefer, B., Rappenglück, B., Flynn, J., Olson, J., and Crawford, J. H.: A Comparison of Chemical Mechanisms Based on Tramp-2006 Field Data, *Atmos. Environ.*, 44, 4116–4125, 2010.
- Creasey, D. J., Heard, D. E., and Lee, J. D.: Eastern Atlantic Spring Experiment 1997 (Ease97) 1. Measurements of OH and HO<sub>2</sub> Concentrations at Mace Head, Ireland, *J. Geophys. Res.*, 107, 10.1029/2001jd000892, 2002.
- Crowley, J. N., Pouvesle, N., Phillips, G. J., Axinte, R., Fischer, H., Petäjä, T., Nölscher, A., Williams, J., Hens, K., Harder, H., Martinez-Harder, M., Novelli, A., Kubistin, D., Bohn, B., and Lelieveld, J.: Insights into HO<sub>x</sub> and RO<sub>x</sub> chemistry in the boreal forest via measurement of peroxyacetic acid, peroxyacetic nitric anhydride (PAN) and hydrogen peroxide, *Atmos. Chem. Phys.*, 18, 13457–13479, 2018.
- Czader, B. H., Li, X., and Rappenglueck, B.: Cmaq Modeling and Analysis of Radicals, Radical Precursors, and Chemical Transformations, *J. Geophys. Res.*, 118, 11,376–311,387, 10.1002/jgrd.50807, 2013.
- Davis, D. D., Rodgers, M. O., Fischer, S. D., and Asai, K.: An Experimental Assessment of the O<sub>3</sub>/H<sub>2</sub>O Interference Problem in the Detection of Natural Levels of OH Via Laser Induced Fluorescence, *Geophys. Res. Lett.*, 8, 69–72, 10.1029/GL008i001p00069, 1981a.

Davis, D. D., Rodgers, M. O., Fischer, S. D., and Heaps, W. S.: A Theoretical Assessment of the O<sub>3</sub>/H<sub>2</sub>O Interference Problem in the Detection of Natural Levels of OH Via Laser Induced Fluorescence, *Geophys. Res. Lett.*, 8, 73-76, 10.1029/GL008i001p00073, 1981b.

Detournay, A., Sauvage, S., Locoge, N., Gaudion, V., Leonardis, T., Fronval, I., Kaluzny, P., and Galloo, J.-C.: Development of a sampling method for the simultaneous monitoring of straightchain alkanes, straight-chain saturated carbonyl compounds and monoterpenes in remote areas, *J. Environ. Monit.*, 13, 983–990, 2011.

Di Carlo, P., Brune, W. H., Martinez, M., Harder, H., Leshner, R., Ren, X., Thornberry, T., Carroll, M. A., Young, V., Shepson, P. B., Riemer, D., Apel, E., and Campbell, C.: Missing OH Reactivity in a Forest: Evidence for Unknown Reactive Biogenic VOCs. *Science*, 304, 5671, 2004.

Dusanter, S., Vimal, D., and Stevens, P. S.: Technical Note: Measuring Tropospheric OH and HO<sub>2</sub> by Laser-Induced Fluorescence at Low Pressure. A Comparison of Calibration Techniques, *Atmos. Chem. Phys.*, 8, 321-340, 2008.

Dusanter, S., Vimal, D., Stevens, P. S., Volkamer, R., and Molina, L. T.: Measurements of OH and HO<sub>2</sub> concentrations during the MCMA-2006 field campaign – Part 1: Deployment of the Indiana University laser-induced fluorescence instrument, *Atmos. Chem. Phys.*, 9, 1665–1685, 2009a.

Dusanter, S., Vimal, D., Stevens, P. S., Volkamer, R., Molina, L. T., Baker, A., Meinardi, S., Blake, D., Sheehy, P., Merten, A., Zhang, R., Zheng, J., Fortner, E. C., Junkermann, W., Dubey, M., Rahn, T., Eichinger, B., Lewandowski, P., Prueger, J., and Holder, H.: Measurements of OH and HO<sub>2</sub> Concentrations During the MCMA-2006 Field Campaign – Part 2: Model Comparison and Radical Budget, *Atmos. Chem. Phys.*, 9, 6655-6675, 2009b.

Dusanter S. and Stevens, P. S.: Recent Advances in the Chemistry of OH and HO<sub>2</sub> Radicals in the Atmosphere: Field and Laboratory Measurements, in *Advances in Atmospheric Chemistry*, Volume 1, John R. Barker, Allison L. Steiner, and Timothy J. Wallington, Editors, World Scientific Publishing Co. Pte. Ltd, New Jersey, pp. 493-579, 2017.

Emmerson, K. M., Carslaw, N., Carpenter, L. J., Heard, D. E., Lee, J. D., and Pilling, M. J.: Urban Atmospheric Chemistry During the Puma Campaign 1: Comparison of Modelled OH and HO<sub>2</sub> Concentrations with Measurements, *J. Atmos. Chem.*, 52, 143-164, 2005.

Emmerson, K. M., Carslaw, N., Carslaw, D. C., Lee, J. D., McFiggans, G., Bloss, W. J., Gravestock, T., Heard, D. E., Hopkins, J., Ingham, T., Pilling, M. J., Smith, S. C., Jacob, M., and Monks, P. S.: Free Radical Modelling Studies During the UK Torch Campaign in Summer 2003, *Atmos. Chem. Phys.*, 7, 167-181, 2007.

Fittschen, C., Al Ajami, M., Batut, S., Ferracci, V., Archer-Nicholls, S., Archibald, A. T., and Schoemaeker, C.: ROOOH: a missing piece of the puzzle for OH measurements in low-NO environments? *Atmos. Chem. Phys.*, 19, 349-362, 2019.

Fuchs, H., Bohn, B., Hofzumahaus, A., Holland, F., Lu, K. D., Nehr, S., Rohrer, F., and Wahner, A.: Detection of HO<sub>2</sub> by Laser-Induced Fluorescence: Calibration and Interferences from RO<sub>2</sub> Radicals, *Atmos. Meas. Tech.*, 4, 1209-1225, 2011.

Fuchs, H., Tan, Z., Hofzumahaus, A., Broch, S., Dorn, H. P., Holland, F., K $\ddot{u}$ nstler, C., Gomm, S., Rohrer, F., Schrade, S., Tillmann, R., and Wahner, A.: Investigation of Potential Interferences in the Detection of Atmospheric RO $_x$  Radicals by Laser-Induced Fluorescence under Dark Conditions, *Atmos. Meas. Tech.*, 9, 1431-1447, 2016.

George, L. A., Hard, T. M., and O'Brien, R. J.: Measurement of Free Radicals OH and HO $_2$  in Los Angeles Smog, *J. Geophys. Res.*, 104, 11643-11655, 10.1029/1998jd100113, 1999.

Goliff, W. S., Stockwell, W. R., and Lawson, C. V.: The Regional Atmospheric Chemistry Mechanism, Version 2, *Atmos. Environ.*, 68, 174-185, 2013.

Griffith, S. M., Hansen, R. F., Dusanter, S., Stevens, P. S., Alaghmand, M., Bertman, S. B., Car-roll, M. A., Erickson, M., Galloway, M., Grossberg, N., Hottle, J., Hou, J., Jobson, B. T., Kammrath, A., Keutsch, F. N., Lefer, B. L., Mielke, L. H., O'Brien, A., Shepson, P. B., Thurlow, M., Wallace, W., Zhang, N., and Zhou, X. L.: OH and HO $_2$  Radical Chemistry During PROPHET 2008 and CABINEX 2009 - Part 1: Measurements and Model Comparison, *Atmos. Chem. Phys.*, 13, 5403-5423, 2013.

Griffith, S. M., Hansen, R. F., Dusanter, S., Michoud, V., Gilman, J. B., Kuster, W. C., Veres, P. R., Graus, M., de Gouw, J. A., Roberts, J., Young, C., Washenfelder, R., Brown, S. S., Thalman, R., Waxman, E., Volkamer, R., Tsai, C., Stutz, J., Flynn, J. H., Grossberg, N., Lefer, B., Alvarez, S. L., Rappenglueck, B., Mielke, L. H., Osthoff, H. D., and Stevens, P. S.: Measurements of Hydroxyl and Hydroperoxy Radicals During CalNex-LA: Model Comparisons and Radical Budgets, *J. Geophys. Res.*, 121, 4211-4232, 10.1002/2015JD024358, 2016.

Hansen, R. F., Griffith, S. M., Dusanter, S., Rickly, P. S., Stevens, P. S., Bertman, S. B., Carroll, M. A., Erickson, M. H., Flynn, J. H., Grossberg, N., Jobson, B. T., Lefer, B. L., and Wallace, H. W.: Measurements of total hydroxyl radical reactivity during CABINEX 2009 – Part 1: field measurements. *Atmos. Chem. Phys.*, 14, 2923-2937, 2014.

Heard, D. E., and Pilling, M. J.: Measurement of OH and HO $_2$  in the Troposphere, *Chem. Rev.*, 103, 5163-5198, 2003.

Hens, K., Novelli, A., Martinez, M., Auld, J., Axinte, R., Bohn, B., Fischer, H., Keronen, P., Kubistin, D., N $\ddot{o}$ lscher, A. C., Oswald, R., Paasonen, P., Pet $\ddot{a}$ j $\ddot{a}$ , T., Regelin, E., Sander, R., Sinha, V., Sipil $\ddot{a}$ , M., Taraborrelli, D., Tatum Ernest, C., Williams, J., Lelieveld, J., and Harder, H.: Observation and Modelling of HO $_x$  Radicals in a Boreal Forest, *Atmos. Chem. Phys.*, 14, 8723-8747, 2014.

Hofzumahaus, A., Rohrer, F., Lu, K., Bohn, B., Brauers, T., Chang, C.-C., Fuchs, H., Holland, F., Kita, K., Kondo, Y., Li, X., Lou, S., Shao, M., Zeng, L., Wahner, A., and Zhang, Y.: Amplified Trace Gas Removal in the Troposphere, *Science*, 324, 1702-1704, 2009.

Holland, F., Hofzumahaus, A., Sch $\ddot{a}$ fer, J., Kraus, A., and P $\ddot{a}$ tz, H.-W.: Measurements of OH and HO $_2$  Radical Concentrations and Photolysis Frequencies During Berlioz, *J. Geophys. Res.*, 108, 8246, doi:8210.1029/2001JD001393, 2003.

Jenkin, M. E., Saunders, S. M., Pilling, M. J. The Tropospheric Degradation of Volatile Organic Compounds: A Protocol for Mechanism Development, *Atmos. Environ.*, 31, 81, 1997.

- Jenkin, M. E., Young, J. C., and Rickard, A. R.: The MCM v3.3.1 degradation scheme for isoprene, *Atmos. Chem. Phys.*, 15, 11433-11459, 2015.
- Kanaya, Y., Sadanaga, Y., Hirokawa, J., Kajii, Y., and Akimoto, H.: Development of a Ground-Based LIF Instrument for Measuring HO<sub>x</sub> Radicals: Instrumentation and Calibrations, *J. Atmos. Chem.*, 38, 73-110, 2001.
- Kanaya, Y., Cao, R., Akimoto, H., Fukuda, M., Komazaki, Y., Yokouchi, Y., Koike, M., Tanimoto, H., Takegawa, N., and Kondo, Y.: Urban Photochemistry in Central Tokyo: 1. Observed and Modeled OH and HO<sub>2</sub> Radical Concentrations During the Winter and Summer of 2004, *J. Geophys. Res.*, 112, 10.1029/2007jd008670, 2007a.
- Kanaya, Y., Cao, R., Kato, S., Miyakawa, Y., Kajii, Y., Tanimoto, H., Yokouchi, Y., Mochida, M., Kawamura, K., and Akimoto, H.: Chemistry of OH and HO<sub>2</sub> Radicals Observed at Rishiri Island, Japan, in September 2003: Missing Daytime Sink of HO<sub>2</sub> and Positive Nighttime Correlations with Monoterpenes, *J. Geophys. Res.*, 112, doi:10.1029/2006JD007987, 2007b.
- Kanaya, Y., Hofzumahaus, A., Dorn, H. P., Brauers, T., Fuchs, H., Holland, F., Rohrer, F., Bohn, B., Tillmann, R., Wegener, R., Wahner, A., Kajii, Y., Miyamoto, K., Nishida, S., Watanabe, K., Yoshino, A., Kubistin, D., Martinez, M., Rudolf, M., Harder, H., Berresheim, H., Elste, T., Plass-Dülmer, C., Stange, G., Kleffmann, J., Elshorbany, Y., and Schurath, U.: Comparisons of Observed and Modeled OH and HO<sub>2</sub> Concentrations During the Ambient Measurement Period of the HO<sub>x</sub>Comp Field Campaign, *Atmos. Chem. Phys.*, 12, 2567-2585, 2012.
- Kim, S., Wolfe, G. M., Mauldin, L., Cantrell, C., Guenther, A., Karl, T., Turnipseed, A., Green-berg, J., Hall, S. R., Ullmann, K., Apel, E., Hornbrook, R., Kajii, Y., Nakashima, Y., Keutsch, F. N., DiGangi, J. P., Henry, S. B., Kaser, L., Schnitzhofer, R., Graus, M., Hansel, A., Zheng, W., and Flocke, F. F.: Evaluation of HO<sub>x</sub> Sources and Cycling Using Measurement-Constrained Model Calculations in a 2-Methyl-3-Butene-2-ol (MBO) and Monoterpene (MT) Dominated Ecosystem, *Atmos. Chem. Phys.*, 13, 2031-2044, 2013.
- Konrad, S., Schmitz, T., Buers, H. J., Houben, N., Mannschreck, K., Mihelcic, D., Müsgen, P., Pätz, H. W., Holland, F., Hofzumahaus, A., Schäfer, H. J., Schröder, S., Volz-Thomas, A., Bächmann, K., Schlomski, S., Moortgat, G., and Großmann, D.: Hydrocarbon Measurements at Pabstthum During the Berlioz Campaign and Modeling of Free Radicals, *J. Geophys. Res.*, 108, 8251, 10.1029/2001jd000866, 2003.
- Kubistin, D., Harder, H., Martinez, M., Rudolf, M., Sander, R., Bozem, H., Eerdekens, G., Fischer, H., Gurk, C., Klüpfel, T., Königstedt, R., Parchatka, U., Schiller, C. L., Stickler, A., Taraborrelli, D., Williams, J., and Lelieveld, J.: Hydroxyl Radicals in the Tropical Troposphere over the Suriname Rainforest: Comparison of Measurements with the Box Model Mecca, *Atmos. Chem. Phys.*, 10, 9705-9728, 2010.
- Kundu, S., Deming, B. L., Lew, M. M., Bottorff, B. P., Rickly, P., Stevens, P. S., Dusanter, S., Sklaveniti, S., Leonardis, T., Locoge, N., and Wood, E. C.: Peroxy Radical Measurements by ethane – nitric oxide chemical amplification and laser-induced fluorescence during the IRRONIC field campaign in a forest in Indiana, *Atmos. Chem. Phys.* 19, 9563-9579, 2019.

Lelieveld, J., Butler, T. M., Crowley, J. N., Dillon, T. J., Fischer, H., Ganzeveld, L., Harder, H., Lawrence, M. G., Martinez, M., Taraborrelli, D., and Williams, J.: Atmospheric Oxidation Capacity Sustained by a Tropical Forest, *Nature*, 452, 737-740, 2008.

Levy, H.: Photochemistry of the Lower Troposphere, *Planetary and Space Science*, 20, 919-935, 1972.

Lew, M. M., Dusanter, S., and Stevens, P. S.: Measurement of Interferences Associated with the Detection of the Hydroperoxy Radical in the Atmosphere Using Laser-Induced Fluorescence, *Atmos. Meas. Tech.*, 11, 95–109, 2018.

Lu, K. D., Hofzumahaus, A., Holland, F., Bohn, B., Brauers, T., Fuchs, H., Hu, M., Häsel, R., Kita, K., Kondo, Y., Li, X., Lou, S. R., Oebel, A., Shao, M., Zeng, L. M., Wahner, A., Zhu, T., Zhang, Y. H., and Rohrer, F.: Missing OH Source in a Suburban Environment near Beijing: Observed and Modelled OH and HO<sub>2</sub> Concentrations in Summer 2006, *Atmos. Chem. Phys.*, 13, 2013.

Mallik, C., Tomsche, L., Bourtsoukidis, E., Crowley, J. N., Derstroff, B., Fischer, H., Hafermann, S., Hüser, I., Javed, U., Keßel, S., Lelieveld, J., Martinez, M., Meusel, H., Novelli, A., Phillips, G. J., Pozzer, A., Reiffs, A., Sander, R., Taraborrelli, D., Sauvage, C., Schuladen, J., Su, H., Williams, J., and Harder, H.: Oxidation processes in the eastern Mediterranean atmosphere: evidence from the modelling of HO<sub>x</sub> measurements over Cyprus, *Atmos. Chem. Phys.*, 18, 10825–10847, 2018.

Mao, J., Ren, X., Zhang, L., Van Duin, D. M., Cohen, R. C., Park, J. H., Goldstein, A. H., Pau-lot, F., Beaver, M. R., Crounse, J. D., Wennberg, P. O., DiGangi, J. P., Henry, S. B., Keutsch, F. N., Park, C., Schade, G. W., Wolfe, G. M., Thornton, J. A., and Brune, W. H.: Insights into Hydroxyl Measurements and Atmospheric Oxidation in a California Forest, *Atmos. Chem. Phys.*, 12, 8009-8020, 2012.

Martinez, M., Harder, H., Kovacs, T. A., Simpas, J. B., Bassis, J., Leshner, R., Brune, W. H., Frost, G. J., Williams, E. J., Stroud, C. A., Jobson, B. T., Roberts, J. M., Hall, S. R., Shetter, R. E., Wert, B., Fried, A., Alicke, B., Stutz, J., Young, V. L., White, A. B., and Zamora, R. J.: OH and HO<sub>2</sub> Concentrations, Sources, and Loss Rates During the Southern Oxidants Study in Nashville, Tennessee, Summer 1999, *J. Geophys. Res.*, 108, 10.1029/2003jd003551, 2003.

Michoud, V., Kukui, A., Camredon, M., Colomb, A., Borbon, A., Miet, K., Aumont, B., Beekmann, M., Durand-Jolibois, R., Perrier, S., Zapf, P., Siour, G., Ait-Helal, W., Locoge, N., Sauvage, S., Afif, C., Gros, V., Furger, M., Ancellet, G., and Doussin, J. F.: Radical Budget Analysis in a Suburban European Site During the Megapoli Summer Field Campaign, *Atmos. Chem. Phys.*, 12, 11951-11974, 2012.

Molina-Herrera, S., Haas, E., Grote, R., Kiese, R., Klatt, S., Kraus, D., Kampffmeyer, T., Friedrich, R., Andreae, H., Loubet, B., Ammann, C., Horváth, L., Larsen, K., Gruening, C., Frumau, A., Butterbach-Bahl, K. Importance of soil NO emissions for the total atmospheric NO<sub>x</sub> budget of Saxony, Germany, *Atmos. Environ.*, 152, 61-76, 2017.

Nölscher, A. C., Yañez-Serrano, A. M., Wolff, S., de Araujo, A. C., Lavrič, J. V., Kesselmeier, J., and Williams, J.: Unexpected seasonality in quantity and composition of Amazon rainforest air reactivity, *Nature Communications*, <https://doi.org/10.1038/ncomms10383>, 2016.

Novelli, A., Hens, K., Tatum Ernest, C., Kubistin, D., Regelin, E., Elste, T., Plass-Dülmer, C., Martinez, M., Lelieveld, J., and Harder, H.: Characterisation of an inlet pre-injector laser-induced fluorescence instrument for the measurement of atmospheric hydroxyl radicals, *Atmos. Meas. Tech.*, 7, 3413-3430, 2014.

Novelli, A., Hens, K., Tatum Ernest, C., Martinez, M., Nölscher, A. C., Sinha, V., Paasonen, P., Petäjä, T., Sipilä, M., Elste, T., Plass-Dülmer, C., Phillips, G. J., Kubistin, D., Williams, J., Vereecken, L., Lelieveld, J., and Harder, H.: Estimating the Atmospheric Concentration of Criegee Intermediates and Their Possible Interference in a FAGE-LIF Instrument, *Atmos. Chem. Phys.*, 17, 7807-7826, 2017.

Peeters, J., Nguyen, T. L., and Vereecken, L.: HO<sub>x</sub> Radical Regeneration in the Oxidation of Isoprene, *Phys. Chem. Chem. Phys.*, 11, 5935, 2009.

Peeters, J., Müller, J.-F., Stavrou, T., and Nguyen, V. S.: Hydroxyl Radical Recycling in Isoprene Oxidation Driven by Hydrogen Bonding and Hydrogen Tunneling: The Upgraded LIM1 Mechanism, *J. Phys. Chem. A*, 118, 8625-8643, 2014.

Reidy, E., Rosales, C., Bottorff, B., Stevens, P. S., Cantrell, C. A., Mauldin, L. Anderson, D. C., and Wood, E. C. D. An Informal Intercomparison of Ambient OH, HO<sub>2</sub>, and RO<sub>2</sub> Measurements in an Indiana Forest Part 2: Comparison with Model Predictions, Abstract A43M-3281 presented at 2018 Fall Meeting, AGU, Washington, D.C., 10-14 Dec., 2018.

Ren, X., Harder, H., Martinez, M., Leshner, R. L., Oliger, A., Simpasa, J. B., Brune, W. H., Schwab, J. J., Demerjian, K. L., He, Y., Zhou, X., and Gao, H.: OH and HO<sub>2</sub> Chemistry in the Urban Atmosphere of New York City, *Atmospheric Environment*, 37, 3639-3651, 2003.

Ren, X., Brune, W., Cantrell, C., Edwards, G., Shirley, T., Metcalf, A., and Leshner, R.: Hydroxyl and Peroxy Radical Chemistry in a Rural Area of Central Pennsylvania: Observations and Model Comparisons, *J. Atmos. Chem.*, 52, 231-257, 2005.

Ren, X., Brune, W. H., Oliger, A., Metcalf, A. R., Simpasa, J. B., Shirley, T., Schwab, J. J., Bai, C., Roychowdhury, U., Li, Y., Cai, C., Demerjian, K. L., He, Y., Zhou, X., Gao, H., and Hou, J.: OH, HO<sub>2</sub>, and OH Reactivity During the PMTACS-NY Whiteface Mountain 2002 Campaign: Observations and Model Comparison, *J. Geophys. Res.*, 111, doi:10.1029/2005JD006126, 2006.

Ren, X., van Duin, D., Cazorla, M., Chen, S., Mao, J., Zhang, L., Brune, W. H., Flynn, J. H., Grossberg, N., Lefer, B. L., Rappenglück, B., Wong, K. W., Tsai, C., Stutz, J., Dibb, J. E., Thomas Jobson, B., Luke, W. T., and Kelley, P.: Atmospheric oxidation chemistry and ozone production: Results from SHARP 2009 in Houston, Texas, *J. Geophys. Res.*, 118, 5770–5780, 2013.

Rickly, P., and Stevens, P. S.: Measurements of the OH Radical Yield from the Ozonolysis of Biogenic Alkenes: A Potential Interference with Laser-Induced Fluorescence Measurements of Ambient OH, *Atmos. Meas. Tech.* 11,1-16, 2018.

Rohrer, F., Lu, K., Hofzumahaus, A., Bohn, B., Brauers, T., Chang, C.-C., Fuchs, H., Haseler, R., Holland, F., Hu, M., Kita, K., Kondo, Y., Li, X., Lou, S., Oebel, A., Shao, M., Zeng, L., Zhu, T., Zhang, Y., and Wahner, A.: Maximum Efficiency in the Hydroxyl-Radical-Based Self-Cleansing of the Troposphere, *Nature Geosci.*, 7, 559-563, 2014.



Rosales, C., Reidy, E., Bottorff, B., Stevens, P. S., Cantrell, C. A., Mauldin, L. Anderson, D. C., and Wood, E. C. D., An Informal Intercomparison of Ambient Measurements of OH, HO<sub>2</sub>, and RO<sub>2</sub> Radicals in an Indiana Forest, Part 1: Comparison of Instrumental Measurements, Abstract A43M-3280 presented at 2018 Fall Meeting, AGU, Washington, D.C., 10-14 Dec., 2018.

Roukos, J., Plaisance, H., Leonardis, T., Bates, M., and Locoge, N.: Development and validation of an automated monitoring system for oxygenated volatile organic compounds and nitrile compounds in ambient air, *J. Chromatr. A*, 1216, 8642–8651, 2009.

Saunders, S. M., Jenkin, M. E., Derwent, R. G., and Pilling, M. J.: Protocol for the development of the Master Chemical Mechanism, MCM v3 (Part A): Tropospheric degradation of non-aromatic volatile organic compounds, *Atmos. Chem. Phys.*, 3, 161-180, 2003.

Sheehy, P. M., Volkamer, R., Molina, L. T., and Molina, M. J.: Oxidative Capacity of the Mexico City Atmosphere – Part 2: A RO<sub>x</sub> Radical Cycling Perspective, *Atmos. Chem. Phys.*, 10, 6993-7008, 2010.

Shetter, R. E., and M. Muller, Photolysis frequency measurements using actinic flux spectroradiometry during the PEM-Tropics mission: Instrumentation description and some results, *J. Geophys. Res.*, 104, 5647–5661, doi:10.1029/98JD01381, 1999.

Shirley, T. R., Brune, W. H., Ren, X., Mao, J., Leshner, R., Cardenas, B., Volkamer, R., Molina, L. T., Molina, M. J., Lamb, B., Velasco, E., Jobson, T., and Alexander, M.: Atmospheric Oxidation in the Mexico City Metropolitan Area (MCMA) During April 2003, *Atmos. Chem. Phys.*, 6, 2753-2765, 2006.

Sklaveniti, S., Locoge, N., Stevens, P. S., Wood, E., Kundu, S., and Dusanter, S.: Development of an instrument for direct ozone production rate measurements: measurement reliability and current limitations, *Atmos. Meas. Tech.*, 11, 741-761, 2018.

Stevens, P. S., Mather, J. H., and Brune, W. H.: Measurement of Tropospheric OH and HO<sub>2</sub> by Laser-Induced Fluorescence at Low Pressure, *J. Geophys. Res.*, 99, 3543-3557, 10.1029/93jd03342, 1994.

Tan, D., Faloona, I., Simpas, J. B., Brune, W., Shepson, P. B., Couch, T. L., Sumner, A. L., Carroll, M. A., Thornberry, T., Apel, E., Riemer, D., and Stockwell, W.: HO<sub>x</sub> Budgets in a Deciduous Forest: Results from the PROPHET Summer 1998 Campaign, *J. Geophys. Res.*, 106, 24407-24427, 10.1029/2001jd900016, 2001.

Tan, Z., Fuchs, H., Lu, K., Hofzumahaus, A., Bohn, B., Broch, S., Dong, H., Gomm, S., Häsel, R., He, L., Holland, F., Li, X., Liu, Y., Lu, S., Rohrer, F., Shao, M., Wang, B., Wang, M., Wu, Y., Zeng, L., Zhang, Y., and Wahner, A.: Radical Chemistry at a Rural Site (Wangdu) in the North China Plain: Observation and Model Calculations of OH, HO<sub>2</sub> and RO<sub>2</sub> Radicals, *Atmos. Chem. Phys.*, 17, 663-690, 2017.

Tan, Z., Rohrer, F., Lu, K., Ma, X., Bohn, B., Broch, S., Dong, H., Fuchs, H., Gkatzelis, G. I., Hofzumahaus, A., Holland, F., Li, X., Liu, Y., Liu, Y., Novelli, A., Shao, M., Wang, H., Wu, Y., Zeng, L., Hu, M., Kiendler-Scharr, A., Wahner, A., and Zhang, Y.: Wintertime photochemistry in Beijing: observations of RO<sub>x</sub> radical concentrations in the North China Plain during the BEST-ONE campaign, *Atmos. Chem. Phys.*, 18, 12391–12411, 2018.

Tan, Z., Lu, K., Hofzumahaus, A., Fuchs, H., Bohn, B., Holland, F., Liu, Y., Rohrer, F., Shao, M., Sun, K., Wu, Y., Zeng, L., Zhang, Y., Zou, Q., Kiendler-Scharr, A., Wahner, A., and Zhang, Y.: Experimental budgets of OH, HO<sub>2</sub>, and RO<sub>2</sub> radicals and implications for ozone formation in the Pearl River Delta in China 2014, *Atmos. Chem. Phys.*, 19, 7129–7150, 2019.

Whalley, L. K., Edwards, P. M., Furneaux, K. L., Goddard, A., Ingham, T., Evans, M. J., Stone, D., Hopkins, J. R., Jones, C. E., Karunaharan, A., Lee, J. D., Lewis, A. C., Monks, P. S., Moller, S. J., and Heard, D. E.: Quantifying the Magnitude of a Missing Hydroxyl Radical Source in a Tropical Rainforest, *Atmos. Chem. Phys.*, 11, 7223-7233, 2011.

Whalley, L. K., Blitz, M. A., Desservettaz, M., Seakins, P. W., and Heard, D. E.: Reporting the Sensitivity of Laser-Induced Fluorescence Instruments Used for HO<sub>2</sub> Detection to an Interference from RO<sub>2</sub> Radicals and Introducing a Novel Approach That Enables HO<sub>2</sub> and Certain RO<sub>2</sub> Types to Be Selectively Measured, *Atmos. Meas. Tech.*, 6, 3425-3440, 2013.

Wolfe, G. M., Marvin, M. R., Roberts, S. J., Travis, K. R., and Liao, J.: The Framework for 0-D Atmospheric Modeling (F0AM) V3.1, *Geosci. Model Dev.*, 9, 3309-3319, 2016.

Zannoni, N., Gros, V., Lanza, M., Sarda, R., Bonsang, B., Kalogridis, C., Preunkert, S., Legrand, M., Jambert, C., Boissard, C., and Lathiere, J.: OH reactivity and concentrations of biogenic volatile organic compounds in a Mediterranean forest of downy oak trees, *Atmos. Chem. Phys.*, 16, 1619-1636, 2016.

Zhou, X., N. Zhang, M. TerAvest, D. Tang, J. Hou, S. Bertman, M. Alaghmand, P. B. Shepson, M. A. Carroll, S. Griffith, S. Dusanter and P. S. Stevens: Nitric acid photolysis on forest canopy surface as a source for tropospheric nitrous acid. *Nature Geosci.*, 4, 440-443, 2011.

**Table 1: Measurements conducted during the IRRONIC field campaign.**

Measurement	Instrument	Technique	LOD	Reference
OH	LIF-FAGE	Laser-induced fluorescence –	$8 \times 10^5 \text{ cm}^{-3} / 30 \text{ min}$	Dusanter et al., 2009a;
HO <sub>2</sub> *		fluorescence assay by gas expansion	$7 \times 10^7 \text{ cm}^{-3} / 20 \text{ s}$	Lew et al., 2018
NO	Thermo 42i-TL	Chemiluminescence	50 ppt / 2 min	
NO <sub>2</sub>	Aerodyne CAPS	Cavity attenuated phase shift spectroscopy	40 ppt / 10 s	
Ozone	2B Technologies Model 202	UV absorbance	3 ppb / 10 s	
OH reactivity	LIF-TOHLM	Total OH Loss Measurement	$1 \text{ s}^{-1}$ (10 min)	Hansen et al., 2013
HONO	LP LIF-FAGE	Laser-photofragmentation laser-induced fluorescence	20 ppt (30 min)	Bottorff et al., in prep
NMHCs	Online GC/FID	Gas chromatography with flame ionization detection	10-100 ppt (1.5 hr)	Badol et al., 2004
OVOCs	Online GC/FID-MS	Gas chromatography with mass spectrometer and FID	5-100 ppt (1.5 hr)	Roukos et al. (2009)
	Off-line Sorbent GC-MS	Sorbent cartridges analyzed by GC-MS		Detournay et al. (2011); Ait-Helal et al. (2014)
	Off-line DNPH HPLC-UV	Dinitrophenylhydrazine cartridges analyzed by high-performance liquid chromatography with UV detection		
J(NO <sub>2</sub> )		Spectral Radiometry	$0.3 \times 10^{-4} \text{ s}^{-1}$	Shetter and Muller (1999)

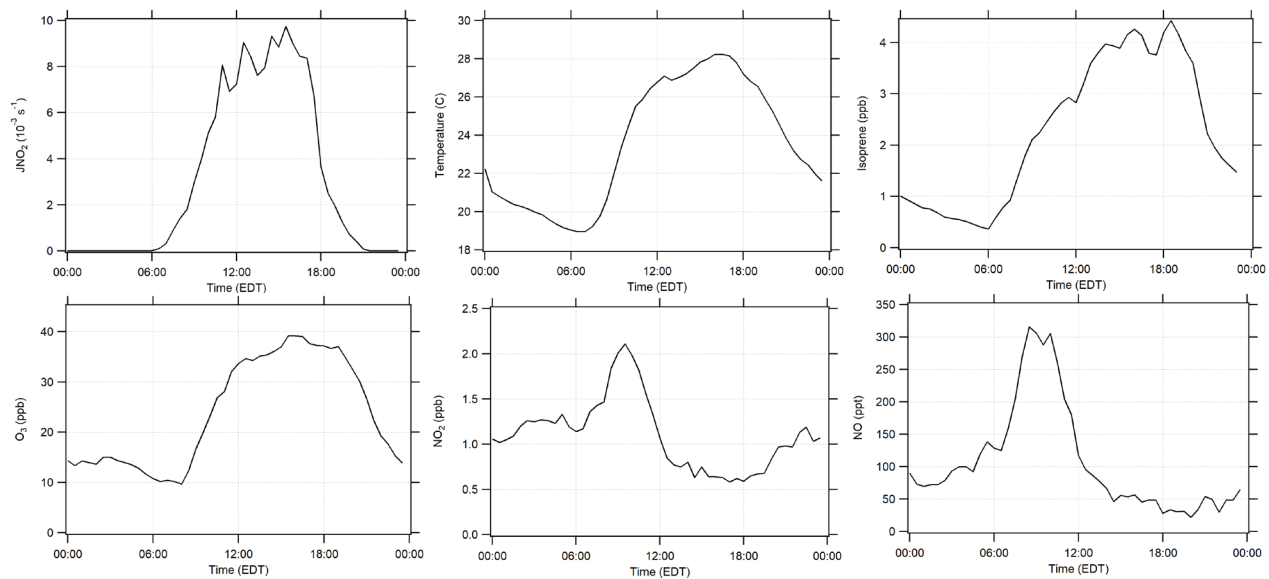


**Figure 1.** Diurnal campaign average profiles of J(NO<sub>2</sub>), temperature, isoprene, O<sub>3</sub>, NO<sub>2</sub>, and NO.

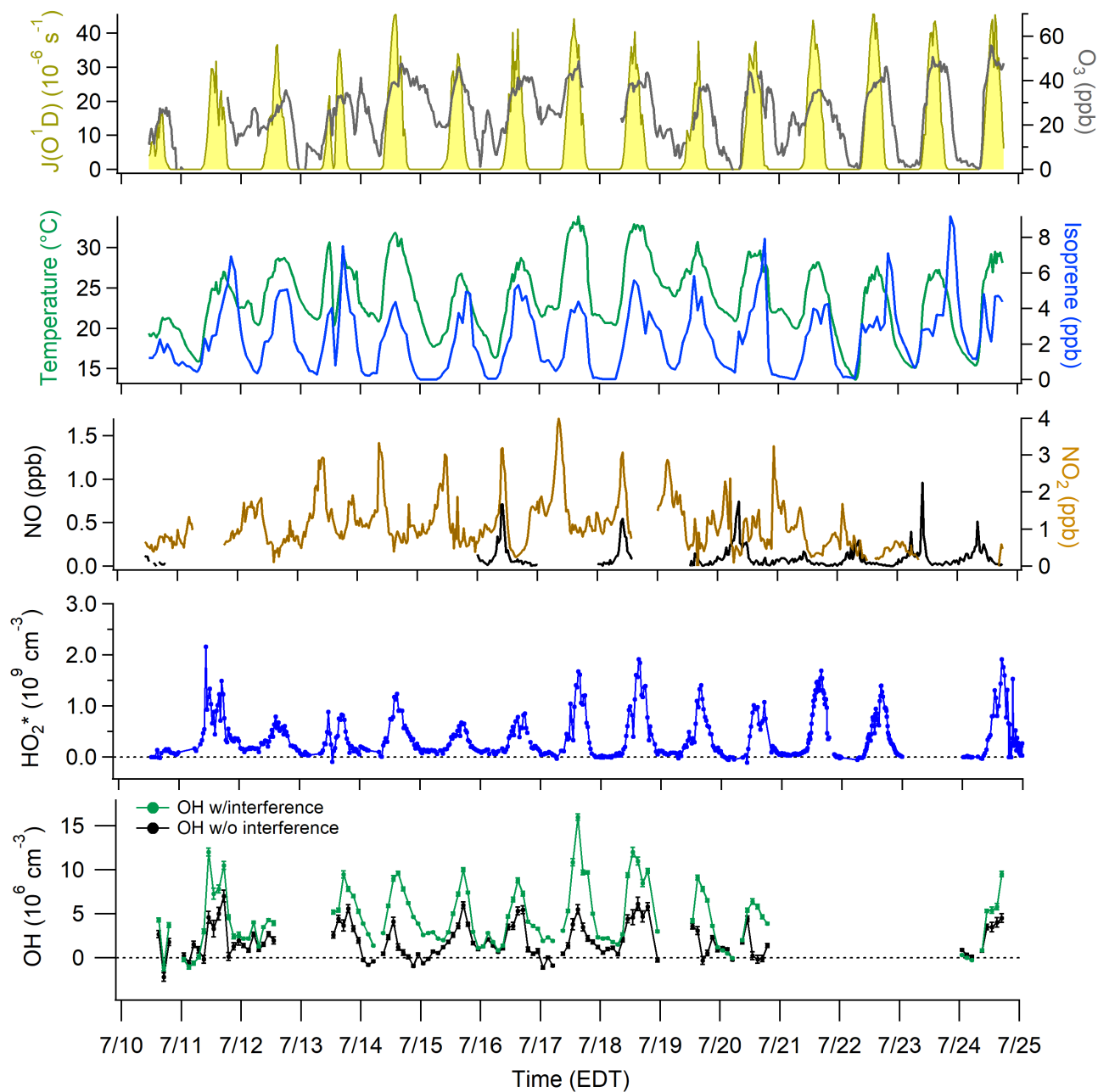


**Figure 2.** Time series of OH and  $HO_2^*$  from July 10 to July 25 with model calculated  $J(O^1D)$  scaled to the measured  $J(NO_2)$ , and measured ozone, temperature, isoprene, and  $NO_x$ . OH measurements with interference ( $\pm 1\sigma$ ) represented by the green line and measurements without interference ( $\pm 1\sigma$ ) represented by the black line. For clarity, OH data shown are 2 hour averages.  $HO_2^*$  data are 30 s averages every 30 minutes.

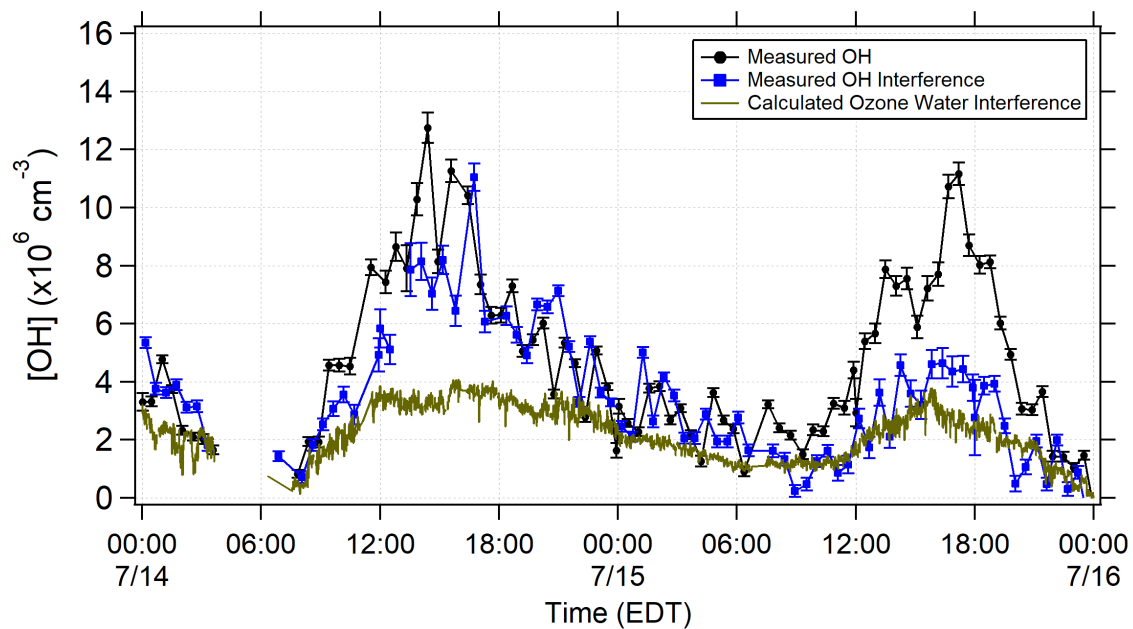


**Figure 3.** Averaged measured total OH signal using spectral modulation (black), and the measured interference using chemical modulation (blue) during July 14 and July 15. The calculated laser-generated interference from ozone photolysis for these days (reactions 1 and 2, green points) is also shown.

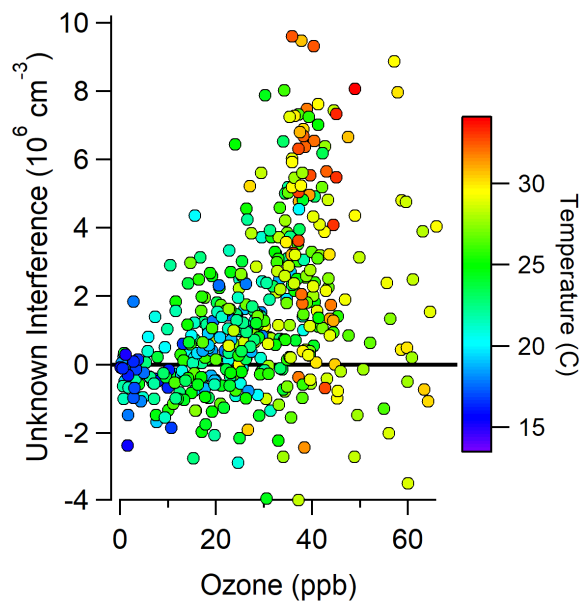


**Figure 4.** Measurements of the unknown interference as a function of ozone and temperature during the campaign.

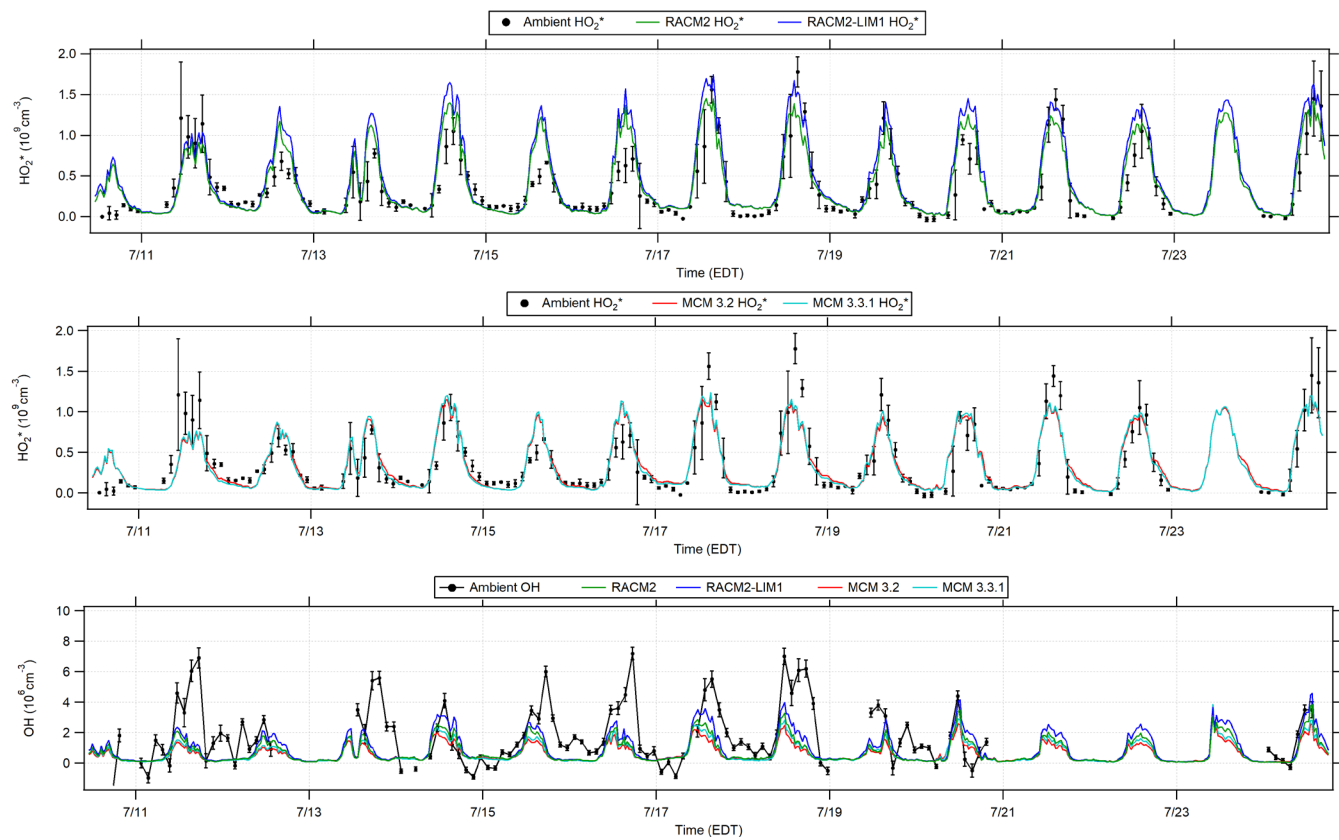


**Figure 5.** Average measurements of  $\text{OH}$  (bottom) and  $\text{HO}_2^*$  from July 10 to July 25 during the IRRONIC campaign in comparison to modeled results for RACM2 and RACM2-LIM1 models (top) and the MCM 3.2 and MCM 3.3.1 models (middle). The error bars represent the precision of the measurements ( $1\sigma$ ).

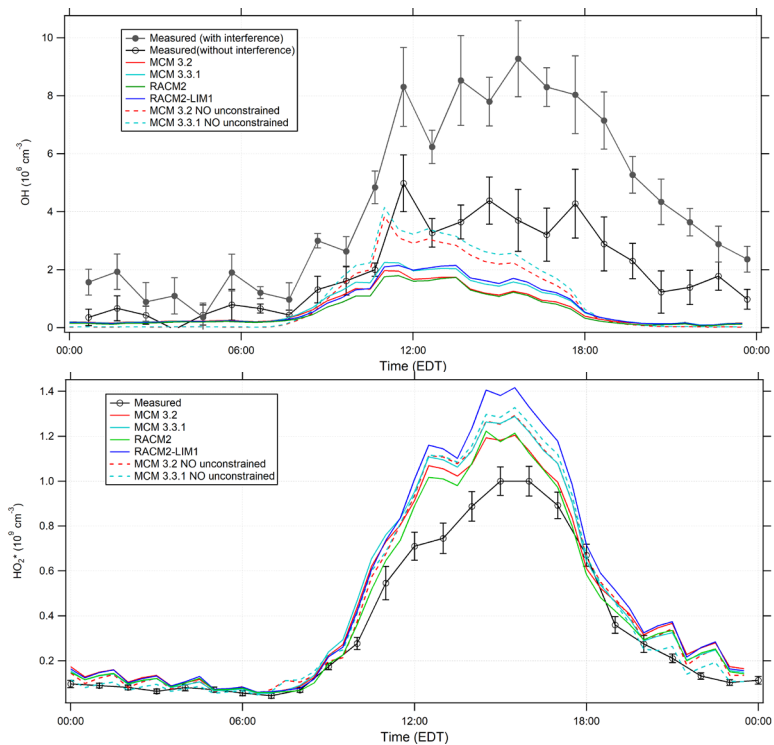


**Figure 6.** Diurnal profiles of OH (top) and  $\text{HO}_2^*$  (bottom) with the RACM2, RACM2-LIM1, MCM 3.2, and MCM 3.3.1 model results. The open circles represent the 1 hour mean  $\pm 1\sigma$  standard error of OH and  $\text{HO}_2^*$  measurements. The filled circles represent the 1 hour mean  $\pm 1\sigma$  standard error of the OH measurements with the interference. The dashed lines represent the MCM 3.2 and 3.3.1 model results with NO concentrations unconstrained (see text).



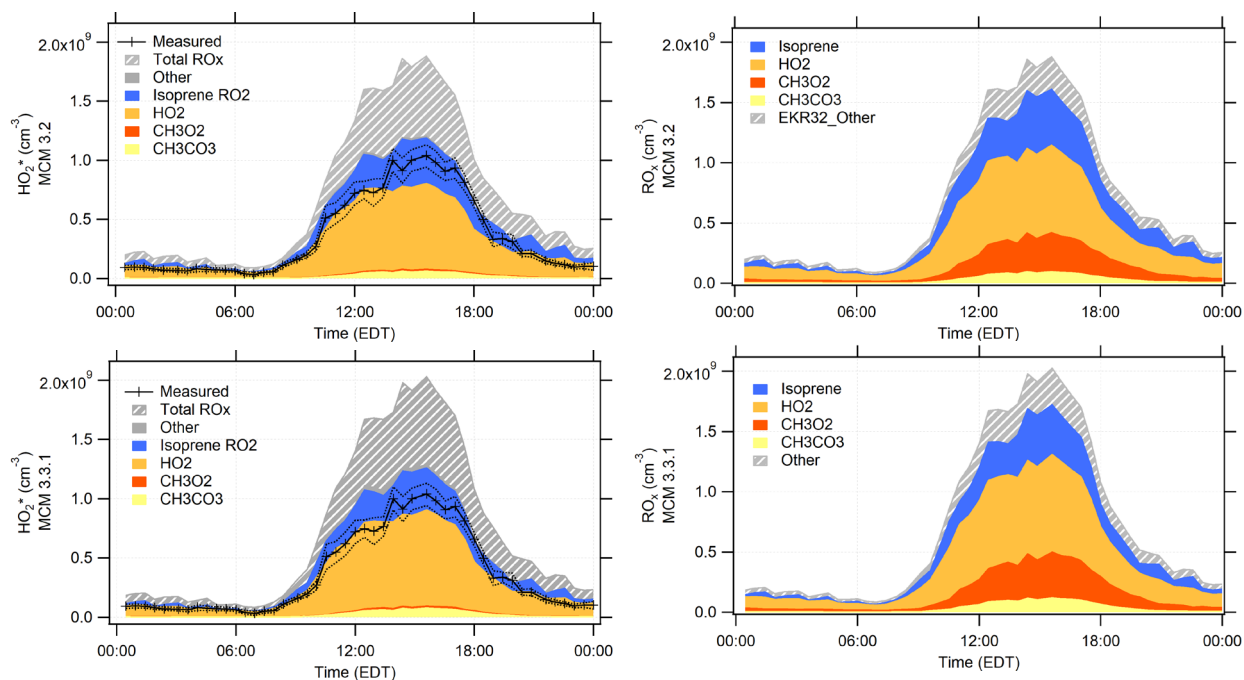


**Figure 7.** The MCM 3.2, and MCM 3.3.1 diurnal average modeled peroxy radical concentration and composition. Left panels show the modeled contribution to the measured  $\text{HO}_2^*$  concentrations. The measured 30-min mean  $\text{HO}_2^*$  concentrations are shown by the black line with  $\pm 1\sigma$  standard error shown by the dotted lines. Right panels show the total  $\text{RO}_x$  ( $\text{RO}_2 + \text{HO}_2$ ) composition predicted by each model.

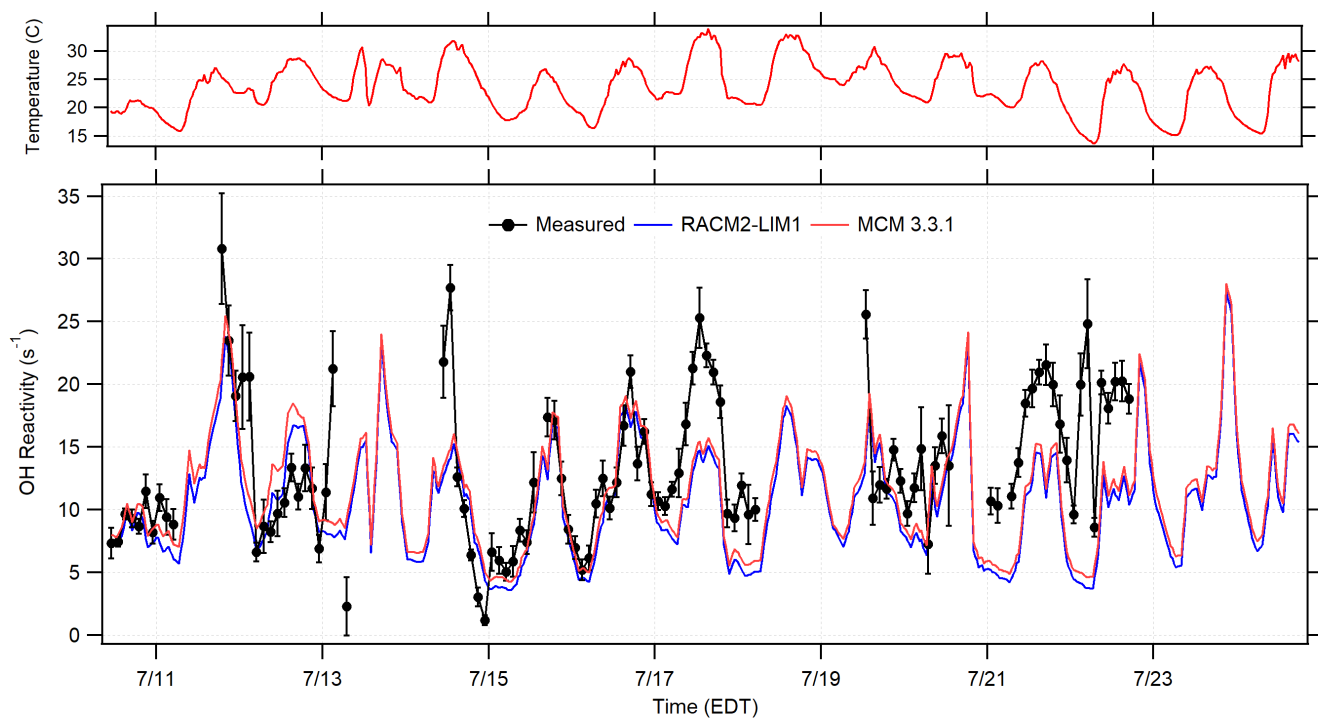


**Figure 8.** Time series of the 2 hour averaged OH reactivity measurements (black circles) in comparison to the RACM2-LIM1 and MCM 3.3.1 calculated OH reactivity based on measured OH sinks along with ambient temperature (top). Error bars represent the standard error of the average measurement.

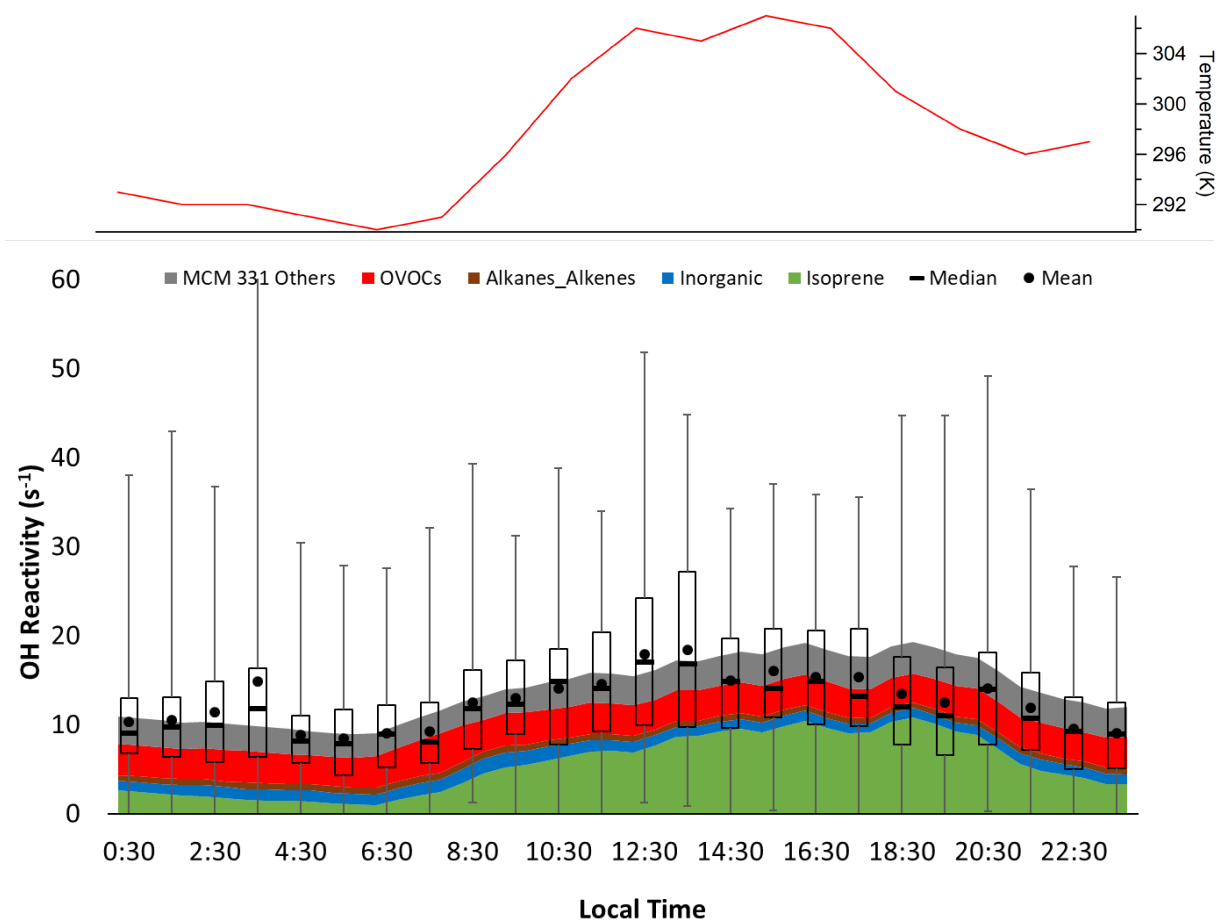


**Figure 9.** Diurnal temperature (top) and box and whiskers plot of observed total OH reactivity showing the mean and median values for each hour, with the mean calculated values from the measured OH sinks as well as the unmeasured oxidation products from the MCM 3.3.1 model results (Others). Error bars show the range of individual 5-min measurements and bars show Q1 and Q3 for the measured OH reactivity.

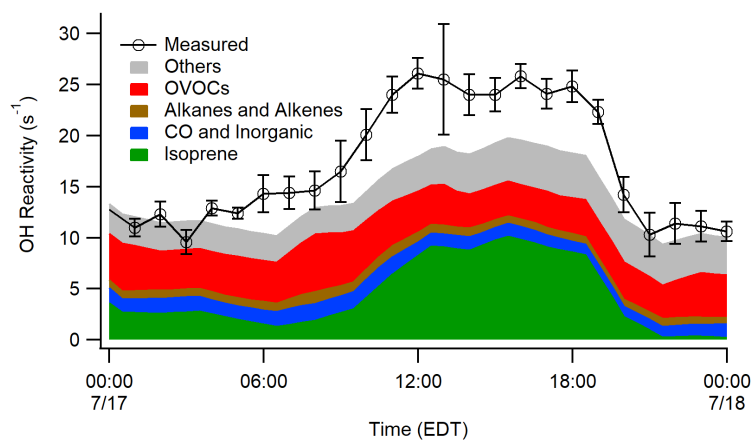


**Figure 10.** Median diurnally averaged OH reactivity from July 17 in comparison to modeled reactivity from the MCM 3.3.1 mechanism.

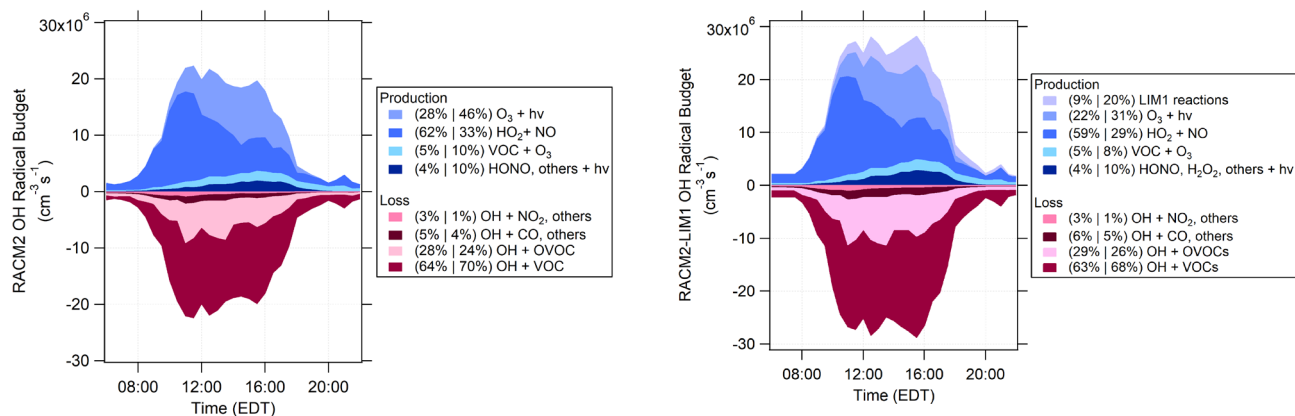


**Figure 11.** RACM2 (left) and RACM2-LIM1 (right) OH radical budgets where the shades of blue represent production reactions and the shades of red represent loss rates. The percent contribution of each reaction to total production/loss are divided into two periods (10:00 to 14:00 and 14:00 to 18:00).

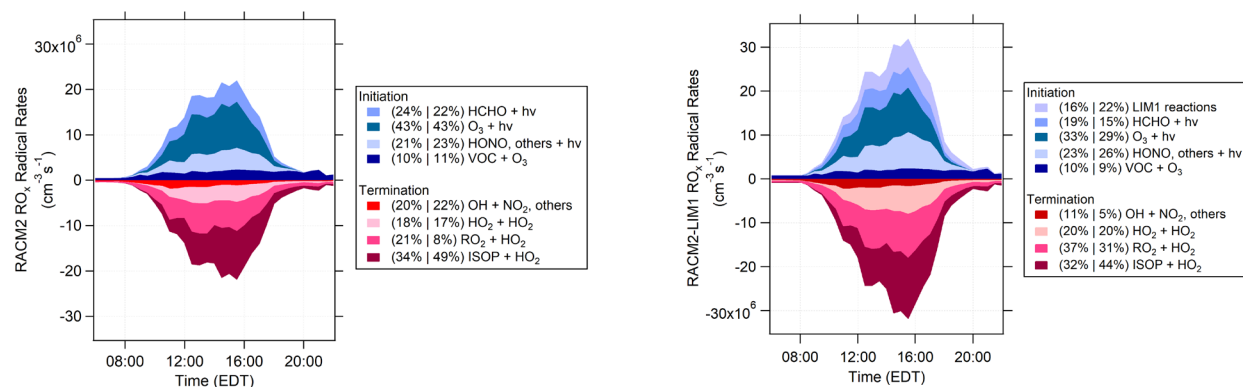


**Figure 12.** RACM2 (left) and RACM2-LIM1 (right) total RO<sub>x</sub> radical budgets where the shades of blue represent initiation rates and the shades of red represent termination rates. The percent contribution of each reaction to total initiation/termination are divided into two periods (10:00 to 14:00 and 14:00 to 18:00).